Geol. Mag. **155** (*6*), *2018, pp. 1377–1393.* © *Cambridge University Press 2017*
doi:10.1017/S0016756817000292

Zircon U–Pb ages and Hf isotope compositions of the Chencai migmatite, central Zhejiang Province, South China: constraints on the early Palaeozoic orogeny

LONGMING LI*†, SHOUFA LIN*‡, JIANHUA LI§, JIAN HE* & YANPENG GE*

*School of Resources and Environment, Hefei University of Technology, Hefei 230026, PR China
‡Department of Earth and Environmental Sciences, University of Waterloo, 200 University Avenue West, Waterloo, Ontario N2L 3G1, Canada
§Institute of Geomechanics, Chinese Academy of Geological Sciences, Beijing 100081, PR China

(*Received* 30 June 2016; *accepted* 28 February 2017; *first published online* 17 April 2017)

Abstract – U–Pb ages and Hf isotope compositions of zircons from the Chencai complex in Zhejiang Province have been determined to provide constraints on mechanisms of migmatization and tectonic evolution related to the early Palaeozoic orogeny in the Cathaysia Block, South China. Zircons from leucosome samples of migmatites are characterized by nebulous overgrowths enclosing inherited cores or occur as newly formed grains with weak zoning. Five samples gave weighted mean ages ranging from 438 ± 3 Ma to 432 ± 4 Ma, which are interpreted as recording the time of anatexis of a regional tectono-thermal event. Their $\varepsilon_{Hf}(t)$ values range from −21.4 to −4.8 (with peak at −11), with corresponding T_{DM2} ages of 1.73–2.77 Ga (with peak at *c.* 1.9–2.3 Ga), suggesting that the protoliths formed by reworking of ancient crust evolved from Late Palaeoproterozoic – early Archaean crust–mantle differentiation. The migmatization was spatially and temporally associated with reported 460–435 Ma metamorphism with a clockwise pressure–temperature (*P*–*T*) path and was most likely controlled by crustal thickening driven by the early Palaeozoic orogenesis. The T_{DM2} ages of the Chencai complex are consistent with those of the Wuyi–Yunkai structural belt in the Cathaysia Block, but distinct from those (with peak at 2.7–3.0 Ga) of the Badu complex which lacks early Palaeozoic tectono-thermal records. The data support the suggestion that a postulated geological entity, instead of the east domain (the Badu complex being its main part) of the Cathaysia Block, was probably involved in the early Palaeozoic orogeny.

Keywords: zircon U–Pb age, Hf isotope, Chencai migmatite complex, early Palaeozoic orogeny, Cathaysia Block.

1. Introduction

During orogenic processes, crustal anatexis shows a close spatial and temporal association with high-grade metamorphism (Williams, Buick & Cartwright, 1996; McLaren, Sandiford & Hand, 1999; Oliver *et al.* 1999; Montero *et al.* 2004; Castiñeiras *et al.* 2008). Crustal anatexis is generally represented by the formation of migmatites or the presence of granitic intrusion. Migmatite commonly consists of mesosomes and leucosomes, with the latter formed by partial melting of high-grade metamorphic assemblages (Brown, 1973, 2001; Sawyer, 2008). The extraction of leucosome from source rocks marks the initiation of crustal anatexis that is commonly followed by leucogranite intrusion (e.g. Johannes *et al.* 2003; Hinchey & Carr, 2006; Alfonso, Raúl & Márcio, 2013). Thus, migmatites, especially the leucosomes, play an important role in understanding the tectonic evolution of large-scale orogenic belts.

The early Palaeozoic orogen in South China is a major orogenic belt in East Asia that formed at a similar time to the classic Caledonian orogeny in Europe (Z. X. Li *et al.* 2010). This early Palaeozoic orogenic belt covers the SE part of the South China Block and extends for *c.* 2000 km in a northeasterly direction (Liu *et al.* 2010*a*). Despite decades of research, there has been no consensus on the tectonic setting and geodynamic mechanism for formation of this orogen (Shu *et al.* 2008; Faure *et al.* 2009; Z. X. Li *et al.* 2010; Y. J. Wang *et al.* 2011, 2012, 2013*b*,*c*; Zhao & Cawood, 2012; Zhang *et al.* 2014*b*; Lin *et al.* 2015). Some researchers emphasize the existence of a Neoproterozoic–Palaeozoic ocean between the Yangtze and Cathaysia blocks and have invoked an early Palaeozoic arc–continent collision following northwestward subduction of the intervening oceanic lithosphere to explain the orogenic event (e.g. Guo, Shi & Lu, 1989; Ma, 2006). However, the validity of this model has been questioned by others due to the absence of early Palaeozoic ophiolite suites, deep-sea sedimentary rocks and arc magmatism (e.g. Shu, 2006; Shu *et al.* 2008; Yi *et al.* 2014). Alternative models, in which the Yangtze and Cathaysia blocks are interpreted to have been amalgamated since the Neoproterozoic, suggest that this orogeny was an intraplate

†Author for correspondence: Longming_li@hfut.edu.cn

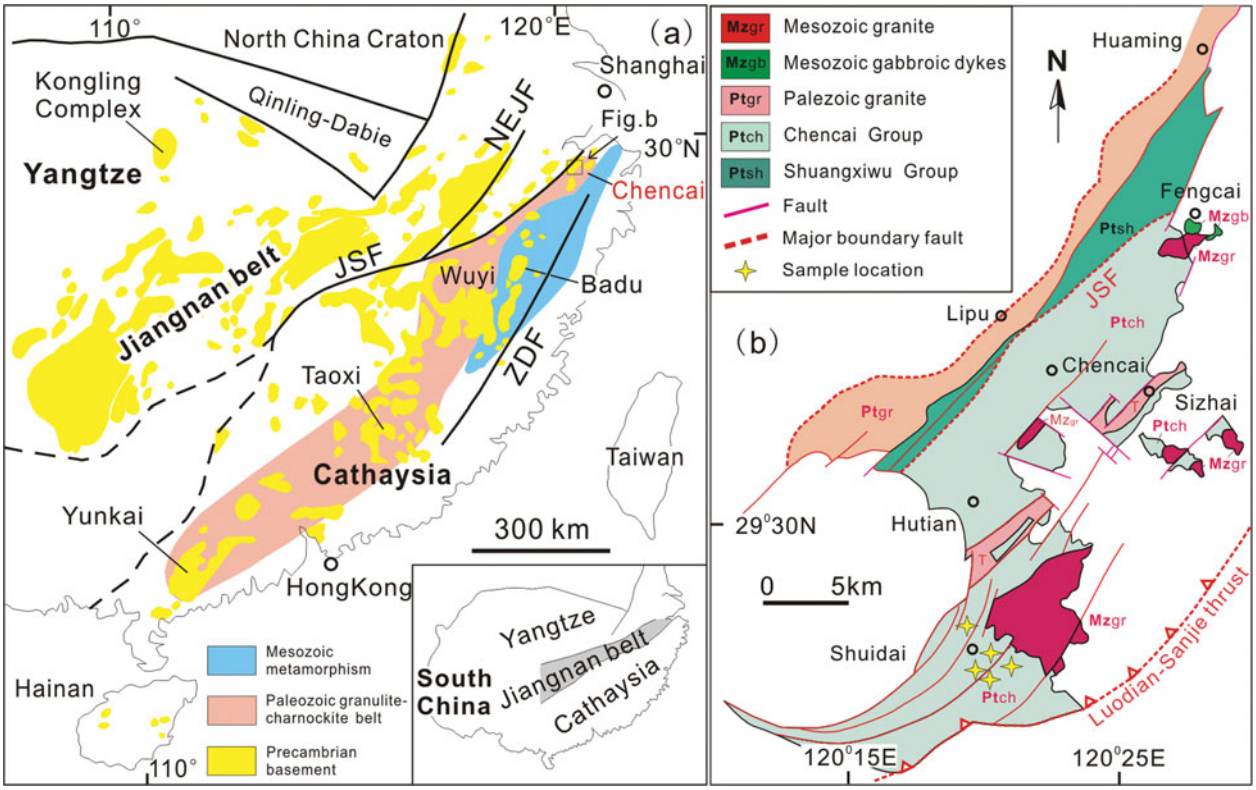

Figure 1. (Colour online) (a) Simplified geological map of South China showing the Precambrian basement. This map is modified after Zhao & Cawood (2012) and Zhao *et al.* (2015b). (b) Simplified geological map of the Chencai region showing the locations of the migmatites.

one (e.g. Charvet *et al.* 1996; Z. X. Li *et al.* 2010; Wang *et al.* 2011; Shu *et al.* 2014; Yu & Shu, 2016), or was a continent–continent collisional event between the Cathaysia Block and a postulated continent that has since moved away from South China (Zhao & Cawood, 2012; Zhang *et al.* 2014*a* ; Chen *et al.* 2015; Lin *et al.* 2015). Previous studies mainly focused on the early Palaeozoic high-grade metamorphism and granitic magmatism (e.g. Wang *et al.* 2011; Zhao *et al.* 2015*b*). Little attention has been paid to the migmatites that occur mostly in the eastern part of this orogen.

In this article, we present U–Pb ages, trace element and Hf isotope compositions of zircons from the migmatites in the Chencai complex in the Cathaysia Block, aiming at providing constraints on the early Palaeozoic orogeny of South China.

2. Geological setting

The South China Block consists of the Yangtze Block in the NW and the Cathaysia Block in the SE, separated by the Jiangshan–Shaoxing fault zone (JSF) (Fig. 1a). The Yangtze Block is considered to have an Archaean–Palaeoproterozoic crystalline basement surrounded by late Mesoproterozoic to early Neoproterozoic folded basement rocks, which are unconformably overlain by Neoproterozoic to Sinian cover sequences (Qiu *et al.* 2000; Zhang *et al.* 2006; Gao *et al.* 2011; L. M. Li *et al.* 2014; J. H. Li *et al.* 2016). The Cathaysia Block mainly consists of Palaeoproterozoic and Neoproterozoic rocks without the occurrence of Archaean rocks (Yu *et al.* 2010, 2012; L. M. Li *et al.* 2011*a*; Xia, Xu & Zhu, 2012; Zheng, Xiao & Zhao, 2013). It is generally believed that the Yangtze Block and the Cathaysia Block were amalgamated along the Jiangnan orogen, with the proposed timing of collision varying from late Mesoproterozoic to middle Neoproterozoic (e.g. X. H. Li *et al.* 2003; Z. X. Li *et al.* 2007; X. L.Wang *et al.* 2007, 2014; W. X. Li *et al.* 2008; L. M. Li *et al.* 2011*b*, 2013*a,b*, 2016; Zhao *et al.* 2011; Y. J. Wang *et al.* 2013a; Dong *et al.* 2015; Zhao, 2015). After the amalgamation, the coherent South China continent underwent significant rifting, generating the Nanhua rift basin (Wang & Li, 2003; Charvet, 2013). The basin was closed by an early Palaeozoic orogenic event, as indicated by a regional angular unconformity at the bottom of upper Devonian, and significant Ordovician to Silurian, magmatism and metamorphism in the Cathaysia Block (e.g. Huang, 1977; Shu *et al.* 1999, 2008; Faure *et al.* 2009; Charvet *et al.* 2010; Liu *et al.* 2010*a*; Z. X. Li *et al.* 2010; L. M. Li *et al.* 2011*c*).

The Chencai complex is located in the northeastern Cathaysia Block (Fig. 1b). The Chencai Group, as the most extensively exposed unit in the complex, is divided into four formations from the base upwards: the Daojiuwan Formation, the Xiahetu Formation, the Xiawuzhai Formation and the Xu'an Formation (Kong *et al.* 1995). It mainly consists of gneiss, garnet–muscovite schist, amphibolites, mafic

https://doi.org/10.1017/S0016756817000292 Published online by Cambridge University Press

Figure 2. (Colour online) Photographs illustrating field occurrence of the migmatites of the Chencai complex.

granulite and marble, and is interpreted as a fore-arc accretionary complex by Gao *et al.* (2011). Previous structural and metamorphic studies indicate that these rocks predominantly dip steeply (>60°) to the SE, and have undergone amphibolite-facies metamorphism and anatexis (Z. X. Li *et al.* 2010; Zhao *et al.* 2015*b*).

Migmatization is pervasive in the Chencai complex. Migmatites for this study were sampled from the Shuidai area (Figs 1b and 2). Most leucosomes are laterally continuous and developed parallel to the gneissic foliation. Some are discontinuously distributed and formed as irregular patches or lenses. A few leucosomes occur at dilatant sites outlining boudin-like patterns. The discontinuous leucosomes and those located at dilatant sites are commonly coarser-grained than leucosomes parallel to the foliation. Their field relationships with country rocks are shown in Figure 2. The mineral assemblages of the migmatites are biotite, quartz, amphibole, plagioclase and garnet (Fig. 3).

3. Analytical methods

Representative samples were selected for zircon U–Pb dating. Zircon concentrates were separated using standard density and magnetic separation techniques. Zircon grains were embedded in a polished epoxy mount and imaged by cathode luminescence (CL). CL images were used to select areas for U–Pb analyses, preferentially targeting primary, uniform crystal domains and avoiding cracks and alteration.

Zircon U–Pb isotopic determination for two samples was performed by Secondary Ion Mass Spectrometry (SIMS) using a CAMECA IMS1280-HR system at the SKLaBIG (State Key Laboratory of Isotope Geochemistry) of the Guangzhou Institute of Geochemistry, Chinese Academy of Sciences. The analytical procedure is similar to that described by X. H. Li *et al.* (2009). A long-term uncertainty of 1.5 % (1 RSD) for $^{206}Pb/^{238}U$ measurements of the standard zircons was propagated to the unknowns (X. H. Li, *et al.*, 2010*a*), although the measured $^{206}Pb/^{238}U$ error in a specific session is generally *c.* 1 % (1 RSD) or less. U and Th concentrations of unknowns were also calibrated relative to the standard zircon Plesovice, with Th and U concentrations of 78 and 755 ppm, respectively (Slama *et al.* 2008). Measured compositions were corrected for common Pb using non-radiogenic ^{204}Pb. Common Pb is very low, and is largely derived from laboratory contamination introduced during sample preparation. An average of present-day crustal composition (Stacey & Kramers, 1975) is used for the common Pb. A secondary standard zircon Qinghu (X. Li *et al.*, 2013*b*) was analysed as unknown to monitor the reliability of

https://doi.org/10.1017/S0016756817000292 Published online by Cambridge University Press

Table 1. Zircon SIMS U–Pb ages for migmatites from Chencai complex in NE Zhejiang province, SE China

			Ratios (common-Pb corrected)					Ages (common-Pb corrected, Ma)						
Grain	U	Th/U	$^{207}Pb/^{235}U$	1σ (%)	$^{206}Pb/^{238}U$	1σ (%)	Err*	$^{207}Pb/^{206}Pb$	±1σ	$^{207}Pb/^{235}U$	±1σ	$^{206}Pb/^{238}U$	±1σ	%Disc
15ZJ9-1														
1	1308	0.11	0.53310	1.4176	0.07009	1.2366	0.8723	419	15	434	5	437	5	4.4
2	1283	0.11	0.52577	1.3908	0.06860	1.2445	0.8948	436	14	429	5	428	5	– 1.9
3	1585	0.06	0.51649	1.4427	0.06752	1.2411	0.8603	432	16	423	5	421	5	– 2.5
4	1105	0.04	0.53120	1.4887	0.06954	1.2414	0.8338	428	18	433	5	433	5	1.2
5	813	0.10	0.51705	1.5115	0.06865	1.2369	0.8183	397	19	423	5	428	5	8.1
6	4611	0.10	0.53841	1.3078	0.06994	1.2364	0.9454	446	9	437	5	436	5	– 2.3
7	1233	0.11	0.52938	1.5598	0.06887	1.2370	0.7930	442	21	431	5	429	5	– 3.1
8	1219	0.06	0.53414	1.4127	0.06991	1.2396	0.8774	429	15	435	5	436	5	1.6
9	980	0.11	0.52820	1.4683	0.06894	1.2365	0.8422	435	18	431	5	430	5	– 1.3
10	910	0.06	0.53051	1.4991	0.07025	1.2404	0.8274	403	19	432	5	438	5	8.9
11	1409	0.05	0.53667	1.3509	0.07074	1.2366	0.9154	413	12	436	5	441	5	6.9
12	3418	0.03	0.57153	1.3008	0.07467	1.2523	0.9628	433	8	459	5	464	6	7.5
13	1207	0.08	0.64932	1.3604	0.07741	1.2363	0.9088	634	12	508	5	481	6	– 25.0
15ZJ11-1														
1	1929	0.05	0.54408	1.0558	0.0708	1.0112	0.9577	443	7	441	4	441	4	– 0.5
2	1552	0.04	0.53926	1.4886	0.0698	1.0578	0.7106	455	23	438	5	435	4	– 4.6
3	2572	0.01	0.55130	3.5671	0.0723	1.0328	0.2895	424	74	446	13	450	4	6.2
4	2675	0.02	0.54918	0.9647	0.0712	0.8788	0.9110	449	9	444	3	444	4	– 1.3
5	1459	0.08	0.53572	1.0092	0.0690	0.9351	0.9266	464	8	436	4	430	4	– 7.5
6	1989	0.02	0.54676	0.9185	0.0708	0.8626	0.9392	453	7	443	3	441	4	– 2.6
7	1346	0.03	0.54205	0.9842	0.0709	0.9034	0.9180	429	9	440	4	442	4	3.1
8	2097	0.01	0.54158	1.7018	0.0703	1.6581	0.9743	446	8	439	6	438	7	– 1.8
9	1495	0.03	0.53934	0.9716	0.0693	0.9030	0.9294	470	8	438	3	432	4	– 8.3
10	1213	0.08	0.53799	1.1941	0.0697	1.1293	0.9457	451	9	437	4	434	5	– 3.8
11	1085	0.10	0.53886	1.1171	0.0699	1.0388	0.9299	450	9	438	4	435	4	– 3.3
12	1834	0.04	0.53471	1.1420	0.0690	1.0777	0.9437	461	8	435	4	430	4	– 6.9

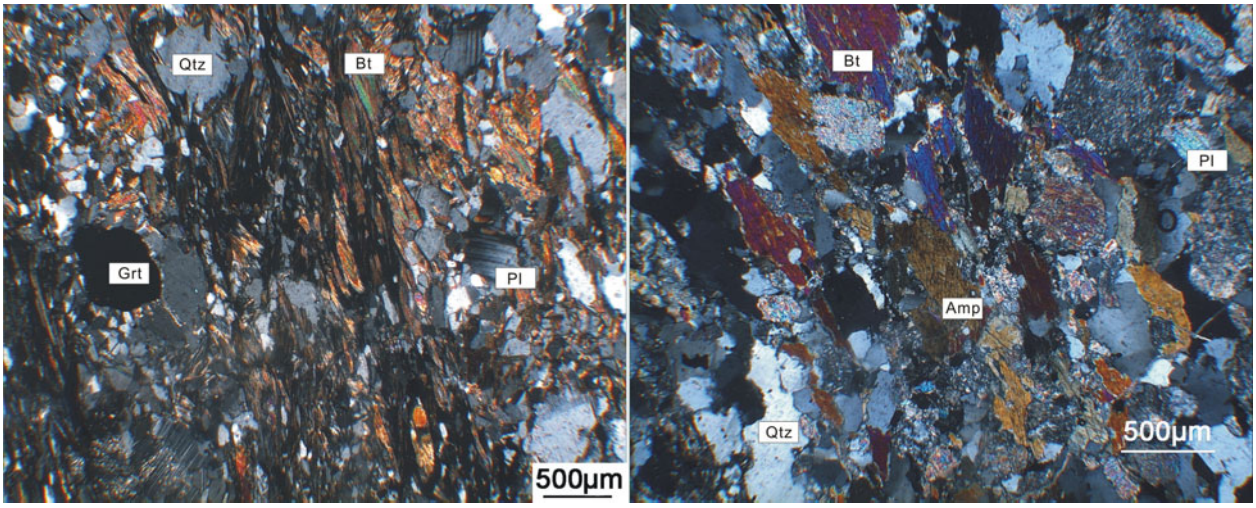

Figure 3. (Colour online) Photomicrographs showing representative mineral assemblages of the migmatites.

the whole procedure. Five analytical spots conducted during the course of this study yield a concordia age of 159.2 Ma, identical to its recommended value. The U–Pb analytical results are given in Table 1. Uncertainties on single analyses are reported at the 1σ level; mean ages for pooled U–Pb analyses are quoted at the 95 % confidence level. Data reduction was carried out using the Isoplot/Ex 3 software (Ludwig, 2003).

Zircon U–Pb isotopic determination for three samples was carried out using laser ablation – inductively coupled plasma – mass spectrometry (LA-ICP-MS) at the School of Resources and Environmental Engineering, Hefei University of Technology (HFUT). A pulsed 193 nm ArF Excimer (COMPex PRO) with laser power of 10 mJ cm^{-2} pulse energy at a repetition ratio of 6 Hz coupled to an Agilent 7500a quadrupole ICP-MS was used for ablation. Helium was used as carrier gas to provide efficient aerosol transport to the ICP and minimize aerosol deposition. The diameter of the laser ablation crater was 32 μm. Zircon 91500 was used as an external standard to normalize isotopic fractionation during isotope analysis. NIST610 glass was used as an external standard to normalize U, Th and Pb concentrations of the unknowns. Meanwhile, standard sample Mud Tank (Black & Culson, 1978) was used as an isotopic monitoring sample. The detailed analytical procedure can be found in Yuan *et al.* (2008). The ICPMS DataCal program (Liu *et al.* 2010*b*) was

https://doi.org/10.1017/S0016756817000292 Published online by Cambridge University Press

used for processing the Pb isotopic data, U–Pb ages and U–Th contents of the zircon analysis spots. Common Pb was corrected according to the method proposed by Anderson (2002). The analytical results are reported with 1σ error (Table 2). The weighted mean U–Pb ages were reported at the 2σ level, and concordia plots were processed using Isoplot/Ex 3 software (Ludwig, 2003).

Hafnium isotopic ratios of zircon measured by multi-collector (MC) LA-MC-ICP-MS at Nanjing FocuMS Technology Co. Ltd. Teledyne Cetac Technologies *Analyte Excite* laser-ablation system (Bozeman, Montana, USA) and Nu Instruments Nu Plasma II MC-ICP-MS (Wrexham, Wales, UK) were combined for the experiments. A193 nm ArF excimer laser, homogenized by a set of beam delivery systems, was focused on the zircon surface with fluence of 6.0 J cm^{-2}. Ablation protocol employed a spot diameter of 50 μm at an 8 Hz repetition rate for 40 s (equating to 320 pulses). Helium was applied as carrier gas to efficiently transport aerosol to MC-ICP-MS. Two standard zircons (including GJ-1, 91500, Plešovice, Mud Tank, Penglai) were treated as quality control every ten unknown samples. The normalizing factor used to correct the mass fractionation of Hf during the measurements is 0.7325 for $^{179}Hf/^{177}Hf$. The reference value of $^{176}Hf/^{177}Hf$ of standard Penglai Zircon is 0.282906 ± 0.000010 (2s) (X. H. Li *et al.* 2010*a*). Analyses of standard Penglai zircon over the measurement period provided $^{176}Hf/^{177}Hf = 0.282926 \pm 0.000016$ (2s) ($n = 6$). Initial $^{176}Hf/^{177}Hf$ values were calculated based on an Lu decay constant of 1.865E−11 (Scherer, Munker & Mezger, 2001). The model ages were computed under the assumption that the $^{176}Lu/^{177}Hf$ of average crust is 0.015, and the $^{176}Hf/^{177}Hf$ and $^{176}Lu/^{177}Hf$ ratios of chondrite and depleted mantle at the present are, respectively, 0.282772 and 0.0332, and 0.28325 and 0.0384 (Blichert-Toft & Albarede, 1997). The analytical results of Hf isotopic compositions are given in Table 3.

4. Results

4.1. Zircon morphology and internal structure

Representative CL images of zircons are shown in Figure 4. Zircons from the leucosomes of the migmatites (samples 15ZJ9-1, 15ZJ11-1) are colourless and transparent. They are euhedral to subhedral and 70–180 μm long with length/width ratios of 1–2. Several grains show core–rim structures with the rims having weak oscillatory zoning. The cores are smaller than their corresponding rims. Most of the newly formed zircons without core display weak oscillatory zoning or nebulous zoning.

Zircon grains from the leucosome of the migmatite (samples 15ZJ4-2, 15ZJ4-5 and 15ZJ4-6) are light purple to transparent, and show morphologies ranging from euhedral, through subhedral to anhedral. Their lengths range from 50 to 150 μm with length/width ratios of 1–3. Some grains have clear core–rim structures with irregular and sharp boundaries. The rims exhibit weak oscillatory zoning, associated with magmatic overgrowth. Some newly formed zircons display no core–rim structures and feature weak oscillatory or planar zoning.

The CL images show that these zircons can be grouped morphologically into two types: (1) grains with concentric, oscillatory zoning; and (2) small cores with wide concentric oscillatory zoned rims. The type 1 zircons and oscillatory-zoned rims in type 2 zircons show a common prismatic morphology with patched, planar or nebulous zoning, both indicative of an igneous origin. The type 2 zircon cores display variously irregular morphologies, and are relicts of older zircons that represent inheritance, presumably from the surrounding country rocks.

4.2. Zircon U–Pb ages

U–Pb dating of samples 15ZJ9-1 and 15ZJ11-1 was performed on the type 1 zircons and the oscillatory-zoned rims in the type 2 zircons by SIMS. A total of 13 zircons from sample 15ZJ9-1 were analysed. Th/U ratios of the zircons range from 0.04 to 0.12. Among these, 11 analyses are concordant and give a weighted mean $^{206}Pb/^{238}U$ age of 432 ± 4 Ma (MSWD = 1.2, $n = 11$) (Fig. 5a). Two analyses gave older $^{206}Pb/^{238}U$ ages of 464 and 480 Ma, respectively. A total of 12 zircons from sample 15ZJ11-1 were analysed. Th/U ratios of the zircons dominantly range from 0.01 to 0.1. Excluding one analysis with a large error, the remaining 11 analyses are concordant and give a weighted mean $^{206}Pb/^{238}U$ age of 437 ± 3 Ma (MSWD = 1.4, $n = 11$) (Fig. 5b).

U–Pb dating of samples 15ZJ4-2, 15ZJ4-5 and 15ZJ4-6 was carried out using LA-ICP-MS. A total of 17 zircons from sample 15ZJ4-2 were conducted, all of which are concordant or nearly concordant. Th/U ratios range from 0.01 to 0.21. One analysis gives a $^{206}Pb/^{238}U$ age of 639 Ma. The remaining 16 analyses are all concordant and give a weighted mean $^{206}Pb/^{238}U$ age of 438 ± 3 Ma (MSWD = 1.7, $n = 16$) (Fig. 5c). Twenty-five analyses were conducted on zircons from sample 15ZJ4-5. Th/U ratios range from 0.02 to 0.22. Twenty-three of the analyses are concordant and give a weighted mean $^{206}Pb/^{238}U$ age of 436 ± 2 Ma (MSWD = 2.1, $n = 23$) (Fig. 5d). A total of 30 zircons from sample 15ZJ4-6 were analysed. Th/U ratios of these zircons dominantly range from 0.06 to 0.46. One analysis gave a $^{206}Pb/^{238}U$ age of 1807 Ma. Excluding two analyses with <95 % concordance, the remaining 27 analyses give a weighted mean $^{206}Pb/^{238}U$ age of 433 ± 2 Ma (MSWD = 2.0, $n = 27$) (Fig. 5e). These zircons have variable Th/U ratios and show steeply rising rare earth elements (REE) patterns with a positive Ce anomaly and clear negative Eu anomaly (Fig. 5), suggesting that they were crystallized from crustal melts.

https://doi.org/10.1017/S0016756817000292 Published online by Cambridge University Press

Table 2. Zircon LA-ICP-MS U–Pb ages for migmatites from Chencai complex

			Ratios (common-Pb corrected)					Ages (common-Pb corrected, Ma)						
Grain	U	Th/U	$^{207}Pb/^{235}U$	1σ	$^{206}Pb/^{238}U$	1σ	Err*	$^{207}Pb/^{206}Pb$	±1σ	$^{207}Pb/^{235}U$	±1σ	$^{206}Pb/^{238}U$	±1σ	%Disc
15ZJ4-2														
1	1159	0.16	0.5436	0.0150	0.0708	0.0007	0.3569	433	63.0	441	9.9	441	4.2	99%
2	381	0.01	0.5363	0.0184	0.0701	0.0008	0.3214	432	88.0	436	12.1	437	4.7	99%
3	898	0.14	0.5027	0.0139	0.0701	0.0007	0.3614	333	66.7	414	9.4	437	4.2	94%
4	2240	0.16	0.5335	0.0126	0.0712	0.0007	0.4048	372	55.6	434	8.4	443	4.1	97%
5	1166	0.10	0.5539	0.0170	0.0700	0.0006	0.2984	498	67.6	448	11.1	436	3.9	97%
6	821	0.16	0.5076	0.0136	0.0706	0.0007	0.3504	287	58.3	417	9.1	440	4.0	94%
7	2057	0.05	0.5085	0.0134	0.0705	0.0007	0.3602	287	58.3	417	9.0	439	4.0	94%
8	943	0.14	0.5196	0.0158	0.0699	0.0006	0.3033	365	68.5	425	10.6	435	3.9	97%
9	656	0.12	0.5511	0.0168	0.0707	0.0007	0.3051	476	68.5	446	11.0	440	4.0	98%
10	1992	0.15	0.5237	0.0121	0.0708	0.0006	0.3697	354	84.3	428	8.0	441	3.6	96%
11	284	0.04	0.9200	0.0265	0.1041	0.0011	0.3750	740	59.3	662	14.0	639	6.6	96%
12	979	0.16	0.5382	0.0116	0.0711	0.0006	0.3694	406	50.0	437	7.7	443	3.4	98%
13	757	0.11	0.5303	0.0140	0.0693	0.0006	0.3199	420	57.4	432	9.3	432	3.5	99%
14	1515	0.20	0.5196	0.0100	0.0690	0.0005	0.3559	387	44.4	425	6.7	430	2.9	98%
15	1011	0.15	0.5359	0.0100	0.0700	0.0005	0.3755	433	38.0	436	6.6	436	3.0	99%
16	1226	0.12	0.5416	0.0107	0.0712	0.0005	0.3575	409	50.0	439	7.0	443	3.0	99%
17	594	0.17	0.5469	0.0129	0.0718	0.0006	0.3320	417	51.8	443	8.5	447	3.4	99%
15ZJ4-5														
1	1381	0.07	0.5350	0.0128	0.0693	0.0006	0.3611	461	56.5	435	8.5	432	3.6	99%
2	2683	0.06	0.5301	0.0120	0.0687	0.0006	0.3648	465	54.6	432	8.0	428	3.4	99%
3	1828	0.10	0.5375	0.0123	0.0694	0.0006	0.3800	476	47.2	437	8.1	433	3.7	99%
4	3112	0.02	0.5339	0.0129	0.0700	0.0006	0.3747	454	65.7	434	8.5	436	3.8	99%
5	3180	0.06	0.5270	0.0140	0.0687	0.0006	0.3369	478	61.1	430	9.3	429	3.7	99%
6	3206	0.02	0.5401	0.0130	0.0700	0.0006	0.3498	480	89.8	439	8.6	436	3.6	99%
7	1237	0.02	0.6827	0.0237	0.0690	0.0006	0.2642	954	73.0	528	14.3	430	3.8	79%
8	1110	0.10	0.5319	0.0126	0.0706	0.0005	0.3266	420	55.6	433	8.4	440	3.3	98%
9	1293	0.08	0.5582	0.0142	0.0705	0.0006	0.3547	524	62.0	450	9.3	439	3.8	97%
10	738	0.13	0.5384	0.0152	0.0696	0.0006	0.3085	465	30.6	437	10.0	434	3.7	99%
11	1634	0.02	0.5348	0.0121	0.0709	0.0006	0.3696	406	53.7	435	8.0	442	3.6	98%
12	2317	0.05	0.5212	0.0113	0.0694	0.0005	0.3439	467	51.8	426	7.5	432	3.1	98%
13	6943	0.02	0.6149	0.0144	0.0732	0.0006	0.3356	650	53.7	487	9.1	455	3.5	93%
14	1169	0.08	0.5221	0.0128	0.0715	0.0006	0.3406	346	91.7	427	8.5	445	3.6	95%
15	1851	0.07	0.5189	0.0123	0.0701	0.0006	0.3554	389	59.3	424	8.2	437	3.6	97%
16	1264	0.22	0.5200	0.0135	0.0712	0.0006	0.3504	367	66.7	425	9.0	444	3.9	95%
17	4412	0.03	0.5111	0.0111	0.0702	0.0005	0.3604	350	55.6	419	7.5	438	3.3	95%
18	1359	0.08	0.5145	0.0120	0.0701	0.0006	0.3440	372	52.8	421	8.0	437	3.4	96%
19	3078	0.03	0.5120	0.0105	0.0700	0.0005	0.3757	369	47.2	420	7.1	436	3.3	96%
20	2142	0.10	0.5149	0.0116	0.0709	0.0006	0.3901	354	55.6	422	7.8	442	3.8	95%
21	682	0.14	0.5437	0.0140	0.0705	0.0007	0.3845	480	63.0	441	9.2	439	4.2	99%
22	1341	0.08	0.5303	0.0123	0.0695	0.0006	0.3825	456	57.4	432	8.2	433	3.7	99%
23	737	0.15	0.5155	0.0137	0.0694	0.0006	0.3103	383	69.4	422	9.2	432	3.5	97%
24	4199	0.03	0.5447	0.0118	0.0723	0.0006	0.4038	406	55.6	442	7.8	450	3.8	98%
25	1168	0.17	0.5208	0.0131	0.0697	0.0006	0.3532	383	61.1	426	8.8	434	3.7	97%
15ZJ4-6														
1	599	0.14	0.5341	0.0155	0.0677	0.0008	0.3857	498	64.8	435	10.3	423	4.6	97%
2	2732	0.21	0.5161	0.0117	0.0692	0.0007	0.4221	365	47.2	423	7.8	431	4.0	98%
3	924	0.18	0.5255	0.0139	0.0680	0.0006	0.3446	443	54.6	429	9.3	424	3.7	98%
4	807	0.14	0.5304	0.0150	0.0707	0.0007	0.3447	389	60.2	432	10.0	440	4.2	98%
5	982	0.06	0.5331	0.0154	0.0687	0.0006	0.3231	450	69.4	434	10.2	429	3.9	98%
6	801	0.13	0.5254	0.0165	0.0703	0.0007	0.3160	369	69.4	429	11.0	438	4.2	97%
7	877	0.12	0.5440	0.0161	0.0705	0.0007	0.3381	435	66.7	441	10.6	439	4.3	99%
8	807	0.13	0.5642	0.0171	0.0716	0.0008	0.3864	476	64.8	454	11.1	446	5.0	98%
9	899	0.13	0.5519	0.0161	0.0694	0.0007	0.3272	502	64.8	446	10.5	432	4.0	96%
10	1078	0.19	0.5468	0.0167	0.0708	0.0007	0.3170	439	68.5	443	11.0	441	4.1	99%
11	1532	0.08	0.5276	0.0152	0.0683	0.0006	0.3220	457	64.8	430	10.1	426	3.8	98%
12	504	0.12	0.5474	0.0168	0.0706	0.0007	0.3330	480	70.4	443	11.0	440	4.4	99%
13	1232	0.19	0.5202	0.0135	0.0684	0.0006	0.3440	439	61.1	425	9.0	426	3.7	99%
14	639	0.14	0.5131	0.0155	0.0698	0.0007	0.3233	369	68.5	420	10.4	435	4.1	96%
15	737	0.15	0.5251	0.0157	0.0703	0.0007	0.3224	409	66.7	429	10.5	438	4.1	97%
16	470	0.11	0.5424	0.0183	0.0688	0.0007	0.3233	524	74.1	440	12.0	429	4.5	97%
17	917	0.15	0.5388	0.0145	0.0703	0.0007	0.3509	454	65.7	438	9.6	438	4.0	99%
18	1690	0.46	1.1135	0.0416	0.0683	0.0008	0.2969	1940	67.1	760	20.0	426	4.6	43%
19	821	0.14	0.5301	0.0162	0.0704	0.0007	0.3146	467	70.4	432	10.8	439	4.1	98%
20	733	0.15	0.5295	0.0178	0.0690	0.0007	0.2975	435	71.3	431	11.8	430	4.2	99%
21	369	0.10	0.5603	0.0223	0.0693	0.0007	0.2464	543	87.0	452	14.5	432	4.1	95%
22	1197	0.21	0.6466	0.0189	0.0700	0.0006	0.2794	833	63.0	506	11.7	436	3.5	85%
23	674	0.12	0.5495	0.0178	0.0691	0.0007	0.3106	506	78.7	445	11.7	431	4.2	96%
24	883	0.17	0.5531	0.0183	0.0701	0.0007	0.2808	487	74.1	447	12.0	437	3.9	97%

https://doi.org/10.1017/S0016756817000292 Published online by Cambridge University Press

Table 2. Continued

Grain	U	Th/U	Ratios (common-Pb corrected)					Ages (common-Pb corrected, Ma)						
			$^{207}Pb/^{235}U$	1σ	$^{206}Pb/^{238}U$	1σ	Err*	$^{207}Pb/^{206}Pb$	±1σ	$^{207}Pb/^{235}U$	±1σ	$^{206}Pb/^{238}U$	±1σ	%Disc
25	697	0.18	0.5486	0.0204	0.0692	0.0007	0.2771	476	87.0	444	13.4	431	4.3	97%
26	640	0.12	0.5293	0.0181	0.0697	0.0007	0.2778	467	77.8	431	12.0	434	4.0	99%
27	662	0.15	0.5391	0.0181	0.0709	0.0009	0.3838	433	81.5	438	12.0	442	5.5	99%
28	902	0.13	0.5411	0.0162	0.0697	0.0007	0.3457	456	66.7	439	10.7	434	4.4	98%
29	870	0.16	0.5156	0.0144	0.0683	0.0006	0.3230	391	68.5	422	9.6	426	3.7	99%
30	278	0.32	7.4970	0.1878	0.3235	0.0031	0.3859	2524	42.9	2173	22.5	1807	15.3	81%

4.3. Zircon Hf isotopes

Because the zircon cores are too small to be simultaneously analysed for trace element and Hf isotope, all Hf isotope analyses were made on newly formed zircon rims. The calculated $\varepsilon_{Hf}(t)$ values and two-stage Hf model ages (T_{DM2}) of the studied zircons are shown in Figure 6.

Sixteen Hf isotope analyses were carried out on 16 zircon grains from sample 15ZJ9-1. The analyses yield consistent $^{176}Hf/^{177}Hf$ ratios between 0.282154 and 0.282296, corresponding to $\varepsilon_{Hf}(t)$ values of −12.4 to −7.3 calculated at $t = 432$ Ma. The T_{DM2} ages are 1.89–2.2 Ga with weighted mean age of 2.02 Ga. Seventeen analyses were made on 17 zircons from sample 15ZJ11-1. The $^{176}Hf/^{177}Hf$ ratios are consistent between 0.282105 and 0.282274. The calculated $\varepsilon_{Hf}(t)$ values are −14 to −8, and the corresponding T_{DM2} ages are 1.94–2.31 Ga (weighted mean of 2.13 Ga) at $t = 437$ Ma.

Twenty-five Hf isotope analyses were carried out on 25 zircon grains from sample 15ZJ4-2. The analyses yield consistent $^{176}Hf/^{177}Hf$ ratios between 0.282122 and 0.28236, corresponding to $\varepsilon_{Hf}(t)$ values of −13.4 to −5 calculated at $t = 438$ Ma. The T_{DM2} ages are 1.74–2.27 Ga with weighted mean of 1.93 Ga. Twenty-five analyses were carried out on 25 zircon grains from sample 15ZJ4-5. The analyses yield consistent $^{176}Hf/^{177}Hf$ ratios between 0.281896 and 0.282292. The calculated $\varepsilon_{Hf}(t)$ values are −21.4 to −7.4, and the corresponding T_{DM2} ages are 1.89–2.77 Ga (weighted mean of 2.33 Ga) at $t = 437$ Ma. Twenty-four Hf isotope analyses were carried out on 24 zircon grains from sample 15ZJ4-6. The analyses yield consistent $^{176}Hf/^{177}Hf$ ratios between 0.282166 and 0.282368, corresponding to $\varepsilon_{Hf}(t)$ values of −11.9 to −4.8 calculated at $t = 433$ Ma. The T_{DM2} ages are 1.73–2.18 Ga (weighted mean age of 1.92 Ga).

5. Discussion

5.1. The early Palaeozoic tectono-thermal sequence of the Chencai complex

Previous geochronological studies on the Chencai complex mainly focused on its protolith age and metamorphic age. The complex was previously regarded as Mesoproterozoic strata (Shui, Xu & Liang, 1986; Shui, 1987; Kong, Bao & Gu, 1994), and a Palaeoproterozoic age has also been obtained (Z. X. Li *et al.* 2010). However, a large amount of recent data indicates that the main part of the Chencai complex formed during the Neoproterozoic (Shu, 2006; Gao, Ding & Liu, 2014; Wang *et al.* 2015).

The metamorphic age of the Chencai complex is also controversial. Geothermobarometrical work suggests multiple episodes of metamorphism from Palaeoproterozoic to Palaeozoic, with a major one in the late Palaeoproterozic (Zhao, Sun & He, 1994). Xu (1987) believed that the major metamorphism occurred in the late Neoproterozoic. This is consistent with the ^{40}Ar–^{39}Ar age (877 ± 10 Ma) of an amphibole (e.g. Kong, Bao & Gu, 1994). However, recent studies show that the amphibolite-facies metamorphism of the Chencai complex happened between *c.* 460 and 435 Ma (Z. X. Li *et al.* 2010; Yao, Shu & Santosh, 2014; Zhao *et al.* 2015*b*).

In this study, five leucosomes from the migmatites in the Chencai complex gave weighted mean ages ranging from 438 ± 3 Ma to 432 ± 4 Ma. Taking into account the CL images of zircons, these ages are interpreted to represent the time of crustal anatexis. Besides the metamorphic rocks and migmatites, several small plutons are also developed in the Chencai complex. A granite and a norite yielded concordant U–Pb ages of 434 ± 4 Ma (Z. X. Li *et al.* 2010) and 422 ± 2 Ma (Zhao *et al.* 2015*b*), respectively.

Metamorphism, migmatization and magmatism are coeval in the Chencai complex and indicate a protracted (~40 Ma) tectono-thermal event lasting from 460 to 420 Ma. Similar results have also been reported for a migmatite complex in the Wuyi–Yunkai structural belt (Y. J. Wang *et al.* 2007; Liu *et al.* 2010*a*; D. Wang *et al.* 2013). These data provide significant constraints on the timing of the early Palaeozoic orogeny, as well as on the metamorphic and magmatic evolution during syn-orogenic crustal thickening (see below).

5.2. Mechanism of migmatization

Different views about the mechanism of migmatization/anatexis have been proposed, including lithosphere thinning accompanied by asthenosphere upwelling (Molnar, Houseman & Conrad, 1998), underplating of basaltic magma (Voshage *et al.* 1990; Dewey, Robb & van Schalkwyk, 2006), decompression by means of exhumation (Whittington &

https://doi.org/10.1017/S0016756817000292 Published online by Cambridge University Press

Table 3. Zircon Lu–Hf isotopic data for the migmatites from Chencai complex

Analysis	Age (Ma)	$^{176}Hf/^{177}Hf$	1σ	$^{176}Lu/^{177}Hf$	1σ	$^{176}Yb/^{177}Hf$	1σ	$^{176}Hf/^{177}Hf$ initial	$\varepsilon_{Hf}(t)$	T_{DM2} (Ga)
15ZJ9-1										
1	432	0.282174	0.000008	0.000352	0.000002	0.017412	0.000034	0.2821708	− 11.8	2.17
2	432	0.282255	0.000006	0.000476	0.000001	0.019873	0.000076	0.2822512	− 8.9	1.99
3	432	0.282293	0.000005	0.000512	0.000004	0.025267	0.000259	0.2822884	− 7.6	1.91
4	432	0.282275	0.000006	0.000428	0.000003	0.019847	0.000167	0.2822718	− 8.2	1.94
5	432	0.282242	0.000006	0.000665	0.000002	0.025541	0.000178	0.2822365	− 9.4	2.02
6	432	0.282243	0.000006	0.000681	0.000002	0.025537	0.000135	0.2822372	− 9.4	2.02
7	432	0.282235	0.000006	0.000442	0.000000	0.021058	0.000058	0.2822315	− 9.6	2.03
8	432	0.282300	0.000006	0.000494	0.000001	0.023387	0.000042	0.2822958	− 7.3	1.89
9	432	0.282161	0.000006	0.000932	0.000019	0.044313	0.001010	0.2821539	− 12.4	2.20
10	432	0.282175	0.000006	0.000779	0.000016	0.035013	0.000563	0.2821683	− 11.9	2.17
11	432	0.282295	0.000006	0.000398	0.000003	0.022857	0.000295	0.2822917	− 7.5	1.90
12	432	0.282257	0.000006	0.000384	0.000002	0.019043	0.000135	0.2822541	− 8.8	1.98
13	432	0.281787	0.000022	0.000473	0.000004	0.020355	0.000281	0.2817831	− 25.5	3.02
14	432	0.282252	0.000006	0.000575	0.000002	0.021610	0.000240	0.2822474	− 9.1	2.00
15	432	0.282257	0.000007	0.000576	0.000012	0.027481	0.000539	0.2822523	− 8.9	1.99
16	432	0.282282	0.000006	0.000428	0.000005	0.022826	0.000196	0.2822784	− 8.0	1.93
15ZJ11-1										
1	437	0.282171	0.000006	0.000677	0.000015	0.036724	0.000593	0.2821651	− 11.9	2.18
2	437	0.282165	0.000006	0.000784	0.000004	0.043882	0.000375	0.2821584	− 12.1	2.19
3	437	0.282188	0.000007	0.000835	0.000007	0.047899	0.000308	0.2821809	− 11.3	2.14
4	437	0.282196	0.000007	0.000757	0.000009	0.040992	0.000597	0.28219	− 11.0	2.12
5	437	0.282165	0.000006	0.000757	0.000008	0.041082	0.000371	0.2821592	− 12.1	2.19
6	437	0.282166	0.000009	0.001095	0.000013	0.056925	0.000713	0.2821566	− 12.2	2.20
7	437	0.282227	0.000007	0.000655	0.000008	0.039207	0.000281	0.2822211	− 9.9	2.05
8	437	0.282268	0.000006	0.000473	0.000007	0.027795	0.000183	0.2822638	− 8.4	1.96
9	437	0.282249	0.000008	0.000338	0.000007	0.021065	0.000387	0.2822466	− 9.0	2.00
10	437	0.282211	0.000007	0.000704	0.000001	0.044497	0.000415	0.2822047	− 10.5	2.09
11	437	0.282198	0.000008	0.000744	0.000004	0.035476	0.000387	0.2821922	− 10.9	2.12
12	437	0.282192	0.000006	0.000542	0.000013	0.030754	0.000614	0.2821872	− 11.1	2.13
13	437	0.282277	0.000008	0.000372	0.000004	0.022765	0.000414	0.2822736	− 8.0	1.94
14	437	0.282148	0.000006	0.000970	0.000001	0.057640	0.000599	0.2821396	− 12.8	2.23
15	437	0.282113	0.000007	0.000943	0.000003	0.058230	0.000384	0.282105	− 14.0	2.31
16	437	0.282151	0.000007	0.000594	0.000017	0.037133	0.001290	0.2821462	− 12.5	2.22
17	437	0.282220	0.000007	0.000500	0.000004	0.030575	0.000505	0.2822159	− 10.1	2.06
15ZJ2-4										
1	438	0.282127	0.000006	0.000560	0.000000	0.027475	0.000291	0.2821223	− 13.4	2.27
2	438	0.282288	0.000006	0.000587	0.000002	0.030497	0.000115	0.2822832	− 7.7	1.91
3	438	0.282336	0.000006	0.000615	0.000001	0.026496	0.000108	0.2823311	− 6.0	1.81
4	438	0.282235	0.000006	0.000860	0.000011	0.035192	0.000547	0.2822283	− 9.6	2.04
5	438	0.282295	0.000006	0.000379	0.000001	0.014858	0.000066	0.2822915	− 7.4	1.89
6	438	0.282366	0.000006	0.000709	0.000002	0.029084	0.000174	0.2823597	− 5.0	1.74
7	438	0.282215	0.000006	0.001251	0.000009	0.046228	0.000092	0.2822051	− 10.4	2.09
8	438	0.282240	0.000006	0.000812	0.000005	0.031631	0.000323	0.2822329	− 9.4	2.03
9	438	0.282359	0.000006	0.000579	0.000005	0.024399	0.000264	0.2823545	− 5.1	1.75
10	438	0.282351	0.000006	0.000494	0.000002	0.024858	0.000146	0.2823472	− 5.4	1.77
11	438	0.282248	0.000007	0.000934	0.000001	0.051519	0.000391	0.2822406	− 9.2	2.01
12	438	0.282324	0.000005	0.000667	0.000001	0.027313	0.000040	0.2823183	− 6.4	1.84
13	438	0.282350	0.000006	0.000487	0.000003	0.023877	0.000222	0.2823461	− 5.4	1.77
14	438	0.282338	0.000006	0.000656	0.000000	0.027322	0.000092	0.2823326	− 5.9	1.80
15	438	0.282216	0.000007	0.001240	0.000004	0.049432	0.000283	0.2822059	− 10.4	2.09
16	438	0.282272	0.000006	0.000799	0.000002	0.034670	0.000109	0.2822654	− 8.3	1.95
17	438	0.282288	0.000008	0.000463	0.000015	0.016015	0.000556	0.2822846	− 7.6	1.91
18	438	0.282243	0.000005	0.000774	0.000002	0.032999	0.000116	0.2822363	− 9.3	2.02
19	438	0.282246	0.000006	0.000841	0.000009	0.033839	0.000464	0.2822386	− 9.2	2.01
20	438	0.282244	0.000006	0.000912	0.000004	0.038147	0.000238	0.2822367	− 9.3	2.02
21	438	0.282355	0.000006	0.000685	0.000004	0.027844	0.000267	0.2823492	− 5.3	1.77
22	438	0.282300	0.000007	0.000341	0.000002	0.018542	0.000247	0.2822968	− 7.2	1.88
23	438	0.282253	0.000007	0.000874	0.000002	0.033839	0.000271	0.2822462	− 9.0	2.00
24	438	0.282236	0.000006	0.000968	0.000007	0.036114	0.000167	0.2822278	− 9.6	2.04
25	438	0.282296	0.000006	0.000725	0.000006	0.027556	0.000298	0.2822902	− 7.4	1.90
15ZJ2-5										
1	437	0.282300	0.000010	0.000962	0.000000	0.031174	0.000257	0.2822924	− 7.4	1.89
2	437	0.281978	0.000011	0.002696	0.000015	0.075917	0.000604	0.2819558	− 19.3	2.64
3	437	0.281978	0.000024	0.002833	0.000012	0.081040	0.000340	0.281955	− 19.3	2.64
4	437	0.282136	0.000010	0.001050	0.000003	0.030560	0.000108	0.2821274	− 13.2	2.26
5	437	0.282155	0.000015	0.001197	0.000004	0.032533	0.000108	0.2821451	− 12.6	2.22
6	437	0.282108	0.000017	0.000970	0.000011	0.027010	0.000375	0.2821003	− 14.2	2.32
7	437	0.282164	0.000008	0.001237	0.000011	0.044643	0.000619	0.2821538	− 12.3	2.20
8	437	0.282110	0.000009	0.001645	0.000014	0.051470	0.000568	0.2820963	− 14.3	2.33
9	437	0.282141	0.000009	0.001198	0.000006	0.039136	0.000376	0.2821315	− 13.1	2.25
10	437	0.282067	0.000008	0.002017	0.000011	0.066712	0.000461	0.2820509	− 15.9	2.43
11	437	0.282164	0.000008	0.001160	0.000001	0.040768	0.000276	0.2821546	− 12.3	2.20
12	437	0.282147	0.000009	0.000820	0.000003	0.026544	0.000167	0.2821407	− 12.8	2.23

https://doi.org/10.1017/S0016756817000292 Published online by Cambridge University Press

Table 3. Continued

Analysis	Age (Ma)	$^{176}Hf/^{177}Hf$	1σ	$^{176}Lu/^{177}Hf$	1σ	$^{176}Yb/^{177}Hf$	1σ	$^{176}Hf/^{177}Hf$ initial	$\varepsilon_{Hf}(t)$	T_{DM2} (Ga)
13	437	0.282114	0.000009	0.001009	0.000005	0.031856	0.000233	0.2821058	− 14.0	2.31
14	437	0.282116	0.000009	0.001194	0.000003	0.040414	0.000336	0.2821065	− 14.0	2.31
15	437	0.281915	0.000012	0.002351	0.000015	0.082765	0.001070	0.2818956	− 21.4	2.77
16	437	0.282127	0.000008	0.000999	0.000009	0.034650	0.000492	0.2821192	− 13.5	2.28
17	437	0.282164	0.000007	0.000735	0.000001	0.036233	0.000234	0.2821578	− 12.1	2.19
18	437	0.282147	0.000006	0.000946	0.000010	0.041090	0.000626	0.2821393	− 12.8	2.23
19	437	0.282140	0.000007	0.000793	0.000003	0.040303	0.000157	0.2821331	− 13.0	2.25
20	437	0.282205	0.000021	0.000761	0.000002	0.030389	0.000194	0.2821988	− 10.7	2.10
21	437	0.282078	0.000007	0.001632	0.000011	0.067423	0.000527	0.2820644	− 15.5	2.40
22	437	0.282011	0.000007	0.001971	0.000009	0.085046	0.000600	0.2819953	− 17.9	2.55
23	437	0.282094	0.000009	0.001843	0.000034	0.078232	0.001880	0.2820792	− 14.9	2.37
24	437	0.282063	0.000006	0.001642	0.000006	0.085238	0.001040	0.2820496	− 16.0	2.43
25	437	0.282002	0.000007	0.002242	0.000007	0.111346	0.000656	0.2819838	− 18.3	2.58
15ZJ2-6										
1	433	0.282263	0.000012	0.000650	0.000005	0.017389	0.000106	0.2822579	− 8.7	1.97
2	433	0.282295	0.000010	0.000962	0.000003	0.028456	0.000151	0.2822875	− 7.6	1.91
3	433	0.282306	0.000010	0.000796	0.000004	0.025913	0.000074	0.2822996	− 7.2	1.88
4	433	0.282319	0.000009	0.000849	0.000009	0.025380	0.000095	0.2823117	− 6.8	1.85
5	433	0.282203	0.000019	0.000605	0.000004	0.017959	0.000068	0.2821981	− 10.8	2.11
6	433	0.282245	0.000013	0.000995	0.000001	0.026751	0.000076	0.2822369	− 9.4	2.02
7	433	0.282309	0.000012	0.000767	0.000003	0.021354	0.000173	0.2823027	− 7.1	1.87
8	433	0.282318	0.000009	0.000779	0.000002	0.026896	0.000245	0.2823113	− 6.8	1.85
9	433	0.282273	0.000010	0.001213	0.000003	0.035312	0.000199	0.2822629	− 8.5	1.96
10	433	0.282301	0.000010	0.000793	0.000005	0.022622	0.000143	0.2822941	− 7.4	1.89
11	433	0.282240	0.000010	0.001388	0.000006	0.037225	0.000269	0.2822289	− 9.7	2.04
12	433	0.282322	0.000012	0.000568	0.000004	0.015765	0.000093	0.2823171	− 6.6	1.84
13	433	0.282267	0.000011	0.001203	0.000003	0.031980	0.000142	0.2822571	− 8.7	1.97
14	433	0.282373	0.000011	0.000544	0.000003	0.018310	0.000277	0.2823683	− 4.8	1.73
15	433	0.282321	0.000013	0.000629	0.000004	0.018464	0.000056	0.2823162	− 6.6	1.84
16	433	0.282316	0.000010	0.000879	0.000004	0.029850	0.000208	0.2823089	− 6.9	1.86
17	433	0.281644	0.000012	0.000400	0.000001	0.011929	0.000132	0.281641	− 30.5	3.33
18	433	0.282268	0.000012	0.001051	0.000006	0.029444	0.000261	0.2822599	− 8.6	1.97
19	433	0.282234	0.000011	0.001400	0.000013	0.041703	0.000418	0.2822226	− 9.9	2.05
20	433	0.282320	0.000010	0.000635	0.000001	0.019791	0.000141	0.2823144	− 6.7	1.85
21	433	0.282328	0.000012	0.000668	0.000002	0.022319	0.000130	0.2823224	− 6.4	1.83
22	433	0.282287	0.000015	0.000447	0.000001	0.011455	0.000030	0.2822836	− 7.8	1.92
23	433	0.282176	0.000010	0.001235	0.000005	0.032431	0.000075	0.2821663	− 11.9	2.18
24	433	0.282237	0.000016	0.000897	0.000013	0.025257	0.000261	0.2822296	− 9.7	2.04

Treloar 2002; Zhang *et al.* 2014*a*), and crustal thickening (Andreoli *et al.* 2006; McLaren *et al.* 2006; Clark *et al.* 2011). In the Cathaysia Block, early Palaeozoic mafic rocks are scare, with only sporadically distributed Silurian gabbros in the Wuyi–Yunkai structural belt and meta-basaltic rocks in the Chencai complex (cf. Y. J. Wang *et al.* 2013*b*; Zhang *et al.* 2015; Zhao *et al.* 2015*b*), precluding the first two mechanisms in explaining the widespread migmatization in the Cathaysia Block. There is also no evidence that rapid exhumation similar to what happened in the Dabie orogen of eastern China (cf. S. J. Wang *et al.* 2013) occurred in the Chencai area and the Wuyi–Yunkai region. We therefore conclude that the migmatization most likely resulted from crustal thickening.

During crustal thickening, the heat may have been produced mainly through the decay of radioactive elements in the buried materials (Y. J. Wang *et al.* 2007; Zhang *et al.* 2012). Progressive heating will induce the breakdown of hydrous minerals to generate initial melts (e.g. Guernina & Sawyer, 2003; Sawyer, 2010; Streule *et al.* 2010; Groppo, Rolfo & Mosca, 2013; Zhang *et al.* 2016). Once the melting of the source rocks had begun, effective viscosity of the middle crust was rapidly lowered and the mechanical strength was significantly reduced, promoting the melt

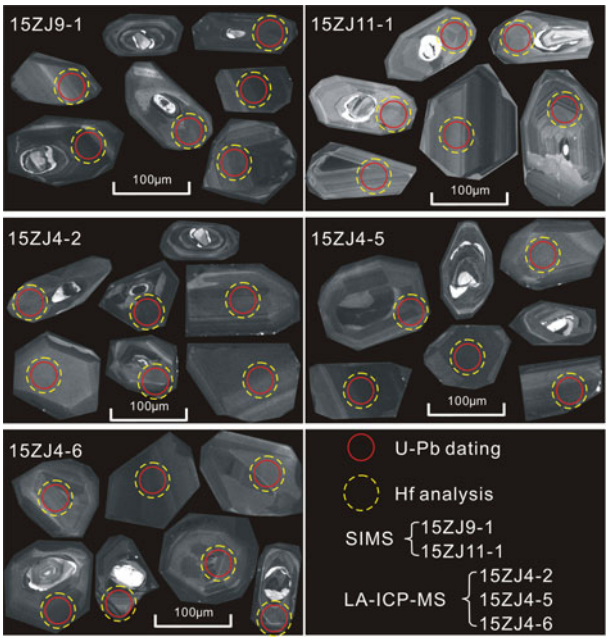

Figure 4. (Colour online) Representative CL images of zircons from the leucosome samples showing morphology and internal structures. The red circles represent the U–Pb analytical spots, and the bigger yellow dashed circles represent the Lu–Hf analytical spots.

https://doi.org/10.1017/S0016756817000292 Published online by Cambridge University Press

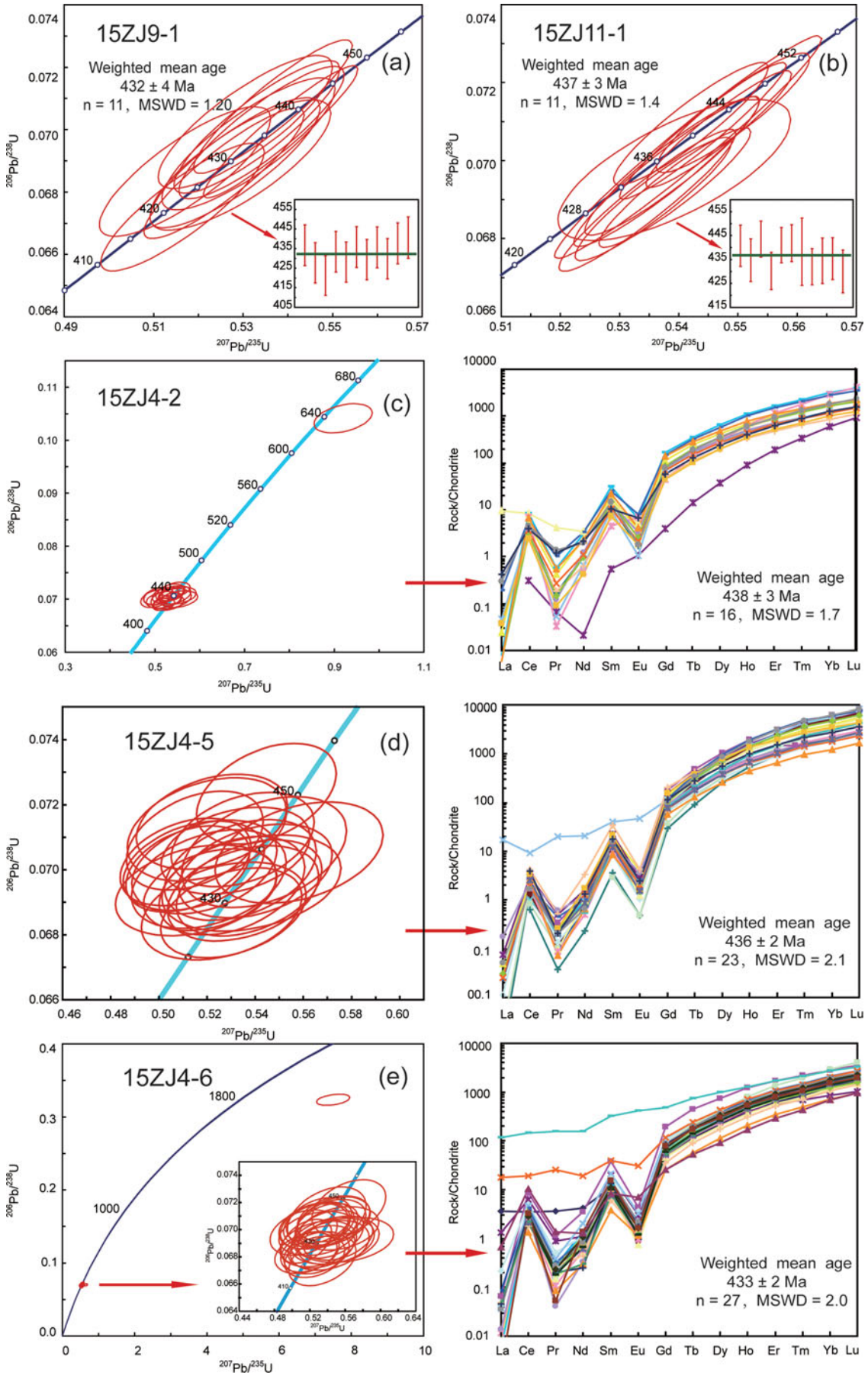

Figure 5. (Colour online) Zircon U–Pb concordia diagrams (a–e) and chondrite-normalized REE patterns. REE normalization factors after Sun & McDonough (1989).

https://doi.org/10.1017/S0016756817000292 Published online by Cambridge University Press

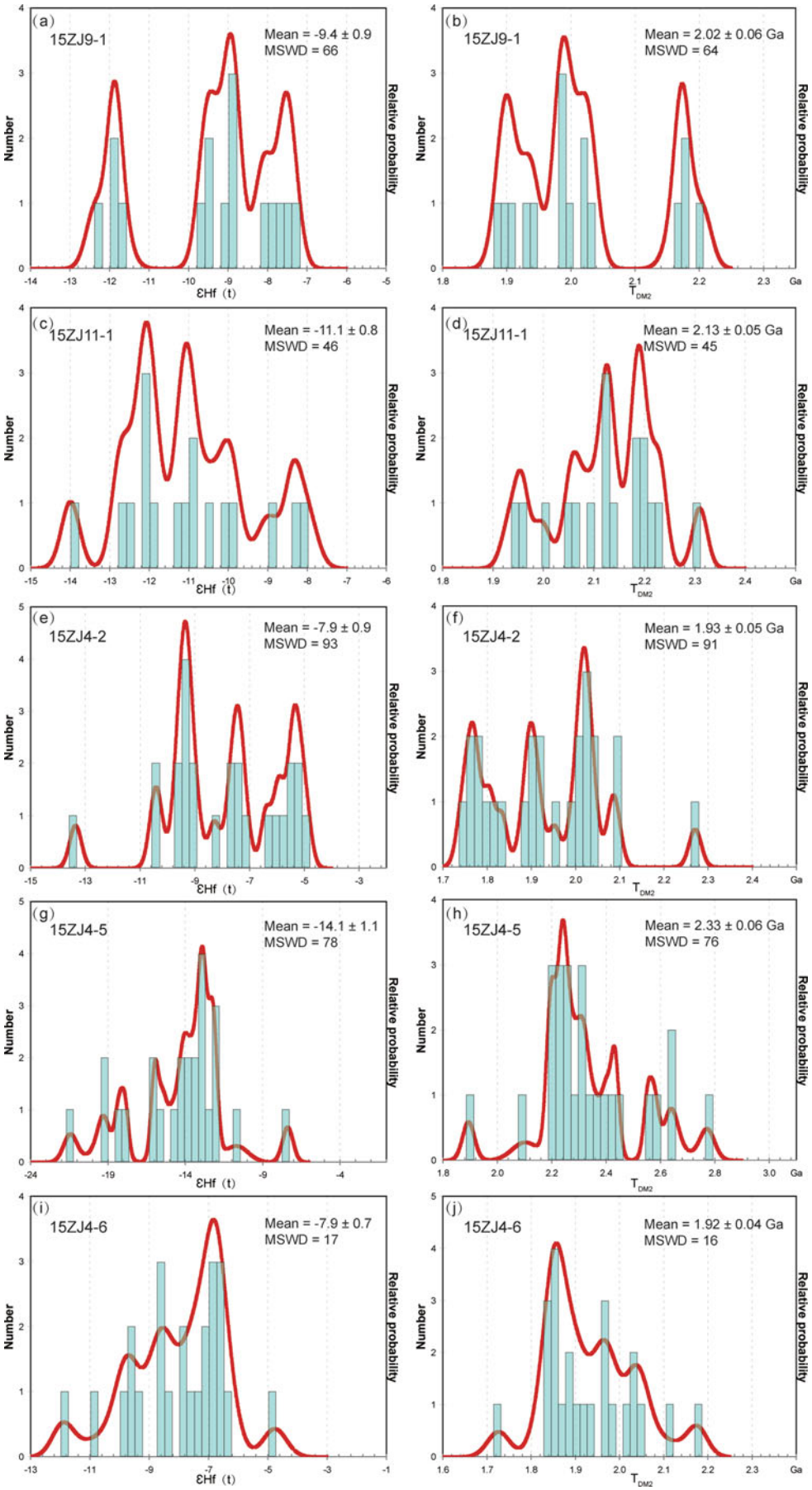

Figure 6. (Colour online) (a–j) Relative probability density diagrams of zircon's $\varepsilon_{Hf}(t)$ values and corresponding two-stage model ages of the studied leucosome samples.

https://doi.org/10.1017/S0016756817000292 Published online by Cambridge University Press

of the crustal materials at the deep level (Brown, 2007; Gerbi, Culshaw & Marsh, 2010; Wang *et al.* 2011; Cottle, Larson & Kellett, 2015). Thus, when the crust was thickened, the thermal budget provided by heat-producing elements could be sufficient to achieve the high-grade metamorphic conditions at middle crustal depths and to induce the generation of granitic melts at deeper crustal levels. Accordingly, migmatization should show a close spatial and temporal association with high grade metamorphism and granitoid emplacement during crustal thickening, which is consistent with the above-mentioned early Palaeozoic sequence of tectono-thermal events in the Chencai complex as well as the Wuyi–Yunkai region.

Notably, the sedimentary protoliths of metapelites experienced amphibolite facies metamorphism in the Chencai complex (Zhao, Sun & He, 1994), requiring significant crustal thickening as these rocks would have been brought down to mid-crustal depths of >20 km to achieve the metamorphic conditions. Zhao & Sun (1994) studied the metamorphic rocks sampled from the Chencai complex and gave peak metamorphic *P–T* conditions of ∼0.7 GPa and ∼550°C and these samples recorded a clockwise *P–T* path. In addition, recent studies also show that the high-grade metamorphic rocks record a near-isothermal decompressional and clockwise *P–T* path in the Wuyi–Yunkai region (Zhao & Cawood, 1999; Yu, Zhou & Zhao, 2003, Yu, Zhou & O'Reilly, 2005; Charvet *et al.* 2010; Z. X. Li *et al.* 2010). Such metamorphic conditions support the idea that the early Palaeozoic metamorphic event in the Chencai complex as well as the Wuyi–Yunkai region was linked to crustal thickening (e.g. Zhao & Sun, 1994; Z. X. Li *et al.* 2010; Wang *et al.* 2011; Zhang *et al.* 2012). We therefore conclude that the migmatization in the Chencai complex was a product of metamorphic evolution, associated with crustal thickening driven by the early Palaeozoic orogeny.

5.3. Tectonic implications

The early Palaeozoic orogeny led to significant crustal reworking of the Cathaysia Block. It has been interpreted as an intraplate orogeny within the SCB (Shu *et al.* 2008; Faure *et al.* 2009; Z. X. Li *et al.* 2010; Y. J. Wang *et al.* 2011, 2012, 2013*a*,*b*), or a continent–continent collisional event that resulted in the region occupied by the present-day southeastern margin (Cathaysia) of SCB colliding with a postulated continental block that later moved away along the Zhenghe–Dapu fault (Zhao & Cawood, 2012; Zhang *et al.* 2014*b*; Lin *et al.* 2015). The early Palaeozoic orogen covers more than half of the area of the Cathaysia Block (Z. X. Li *et al.* 2010), and an understanding of its evolution needs to consider the nature of the basement in the Cathaysia Block.

Recent studies show that the Cathaysia Block is likely composed of two different domains (i.e. west and east Cathaysia), although the exact boundary is unclear (Xu *et al.* 2007; Y. J. Wang *et al.* 2013a; Zhang *et al.* 2014*b*). Such a division is supported by zircon U–Pb dating and Hf isotopic data from different areas of the Cathaysia Block including the Yunkai, Nanling and Wuyi areas as well as the Badu area (e.g. Xu *et al.* 2007). The early Palaeozoic zircons of the Yunkai charnockites and gneissic migmatites yielded $\varepsilon_{Hf}(t) = -16.2$ to -3.5 and T_{DM2} ages of 1.7–2.4 Ga (with peak at *c.* 1.8–2.1 Ga) (D. Wang *et al.* 2013*b*). Similarly, the T_{DM2} ages of the Nanling area, indicated by zircons from the Jurassic, Triassic and Ordovician granitic plutons, range from 1.6 to 2.2 Ga (Shu *et al.* 2013). These suggest ancient crust evolved from Palaeoproterozoic crust–mantle differentiation. The T_{DM2} ages of the studied migmatites in the Chencai complex also reflect a major episode of crustal growth in Palaeoproterozoic time (*c.* 1.9–2.3 Ga), indicating that the Chencai complex may represent the NE extension of the Wuyi–Yunkai structural belt. In contrast, zircons from the Badu complex yield T_{DM2} ages clustering between 2.4 and 3.0 Ga (with the peak at 2.7–3.0 Ga) (Yu *et al.* 2009; Zhao *et al.* 2014, 2015*a*), suggesting that a major crustal growth took place during Archaean time.

The zircon Hf data summarized above suggest that the Chencai–Wuyi–Yunkai region (referred to as the main part of the west Cathaysia domain) exhibits a crustal growth history different from the Badu area (referred to as the main part of the east Cathaysia domain). In addition to the distinct crustal growth processes, the two domains display different tectonic evolution histories. The west domain experienced the early Palaeozoic tectono-thermal event, whereas the east domain was predominantly affected by Mesozoic (250–230 Ma) metamorphic reworking (Xiang *et al.* 2008; Yu *et al.* 2009; Zhao *et al.* 2014). By considering the contrast in geological history between the two domains, Lin *et al.* (2015) suggest that they might not have amalgamated until the Mesozoic. They further suggest that the early Palaeozoic orogeny was a result of a continent–continent collision between the west Cathaysia domain and a postulated separate continent to the east (instead of the east Cathaysia domain) that moved away from South China through later rifting and/or strike-slip motion (Lin *et al.* 2015). Orogen-parallel large-scale strike-slip motion is common in many orogenic belts (e.g. the Canadian Appalachians; Lin *et al.* 2013).

Collectively, our new results on the migmatites of the Chencai complex provide alternative solutions for the geodynamic mechanism of the early Palaeozoic orogeny, and help to improve understanding of the crustal growth and early Palaeozoic tectonic evolution of the Cathaysia Block.

6. Conclusions

1. Migmatization in the Chencai complex took place during *c.* 438–432 Ma.

2. The migmatization was associated with crustal thickening driven by the early Palaeozoic orogeny.

https://doi.org/10.1017/S0016756817000292 Published online by Cambridge University Press

3. Hf isotopic data of zircons from the Chencai complex are similar to those of the Wuyi–Yunkai region, but different from those of the Badu region. The latter also lacks evidence for an early Palaeozoic tectono-thermal event. This supports the idea that the early Palaeozoic orogeny was a result of collision of the west Cathaysia domain with a postulated continent (instead of the east Cathaysia domain).

Acknowledgements. This paper greatly benefited from the comments of two anonymous reviewers. This work was financially supported by China NSFC grant (41573023). The Research Funding for Young Huangshan Scholar of HFUT to Longming Li is gratefully acknowledged. X. P. Xia and Q. Z. Li are thanked for zircon SIMS and LA-ICP-MS U–Pb dating, respectively. We also thank L. Qi for major and trace element analyses and J. F. Gao for Hf isotopic analyses.

References

Alfonso, M. S., Raúl, A. B. & Márcio, M. P. 2013. Petrogenesis of migmatites and leucogranites from Sierra de Molinos, Salta, Northwest Argentina: a petrologic and geochemical study. *Lithos* **177**, 470–91.

Anderson, T. 2002. Correction of common lead in U-Pb analyses that do not report ^{204}Pb. *Chemical Geology* **192**, 59–79.

Andreoli, M. A, Hart, R. J, Ashwal, L. D. & Coetzee, H. 2006. Correlations between U, Th content and metamorphic grade in the Western Namaqualand belt, South Africa, with implication for radioactive heating of the crust. *Journal of Petrology* **47**, 1095–118.

Black, L. P. & Culson, B. L. 1978. The age of the Mud Tank carbonatite, Strangways Range, Northern Territory. *BMR Journal of Australian Geology & Geophysics* **3**, 227–32.

Blichert-Toft, J. & Albarede, F. 1997. The Lu-Hf isotope geochemistry of chondrites and the evolution of the mantle-crust system. *Earth and Planetary Science Letters* **148**, 243–58.

Brown, M. 1973. The definition of metatexis, diatexis and migmatite. *Proceedings of the Geologists' Association* **84**, 371–82.

Brown, M. 2001. Orogeny, migmatites and leucogranites: a review. *Proceedings of the Indian National Science Academy* **110**, 313–36.

Brown, M. 2007. Crustal melting and melt extraction, ascent and emplacement in orogens: mechanisms and consequences. *Journal of the Geological Society* **164**(4), 709–30.

Castiñeiras, P., Villaseca, C., Barbero, L. & Martín Romera, C. 2008. SHRIMP U-Pb zircon dating of anatexis in high-grade migmatite complexes of Central Spain: implications in the Hercynian evolution of Central Iberia. *International Journal of Earth Sciences* **97**(1), 35–50.

Charvet, J. 2013. The Neoproterozoic–Early Paleozoic tectonic evolution of the South China Block: an overview. *Journal of Asian Earth Sciences* **74**, 198–209.

Charvet, J., Shu, L. S., Faure, M., Choulet, F., Wang, B., Lu, H. F. & Breton, N. L. 2010. Structural development of the Lower Paleozoic belt of South China: genesis of an intracontinental orogen. *Journal of Asian Earth Sciences* **39**, 309–30.

Charvet, J., Shu, L. S., Shi, Y. S., Guo, L. Z. & Faure, M. 1996. The building of South China: collision of Yangzi and Cathaysia blocks, problems and tentative answers. *Journal of Southeast Asian Earth Sciences* **13**, 223–35.

Chen, X. Y, Tong, L. X., Zhang, C. L, Zhu, Q. B. & Li, Y. N. 2015. Retrograde garnet amphibolite from eclogite of the Zhejiang Longyou area: new evidence of the Caledonian orogenic event in the Cathaysia block. *Science Bulletin* **60**(13), 1207–17 (in Chinese with English summary).

Clark, C., Fitzsimons, I. C., Healy, D. & Harley, S. L. 2011. How does the continental crust get really hot? *Elements* **7**, 235–40.

Cottle, J. M., Larson, K. P. & Kellett, D. A. 2015. How does the mid-crust accommodate deformation in large, hot collisional orogens? A review of recent research in the Himalayan orogen. *Journal of Structural Geology* **78**, 119–33.

Dewey, J. F., Robb, L. & van Schalkwyk, L. 2006. Did bushmanland extensionally unroof Namaqualand? *Precambrian Research* **150**, 173–82.

Dong, S. W., Zhang, Y. Q., Gao, R., Su, J. B., Liu, M. & Li, J. H. 2015. A possible buried Paleoproterozoic collisional orogen beneath central South China: evidence from seismic-reflection profiling. *Precambrian Research* **264**, 1–10.

Faure, M., Shu, L. S., Wang, B., Charvet, J., Choulet, F. & Monié, P. 2009. Intracontinental subduction: a possible mechanism for the Early Palaeozoic Orogen of SE China. *Terra Nova* **21**, 360–8.

Gao, L. Z., Ding, X. Z. & Liu, Y. X. 2014. SHRIMP zircon U-Pb dating of Neoproterozoic Chencai Complex in Jiangshan-Shaoxing fault zone and its implication. *Geological Bulletin of China* **33**(5), 641–8 (in Chinese with English summary).

Gao, S., Jie, Y., Lian, Z., Li, M., Hu, Z. C., Guo, J. L., Yuan, H. L., Gong, H. J., Xiao, G. Q. & Wei, J. Q. 2011. Age and growth of the Archean Kongling terrain, south China, with emphasis on 3.3 Ga granitoid gneisses. *American Journal of Science* **311**, 153–82.

Gerbi, C., Culshaw, N. G. & Marsh, J. H. 2010. Magnitude of weakening during crustal-scale shear zone development. *Journal of Structural Geology* **32**, 107–17.

Groppo, C., Rolfo, F. & Mosca, P. 2013. The cordierite-bearing anatectic rocks of the higher Himalayan crystallines (eastern Nepal): low-pressure anatexis, melt productivity, melt loss and the preservation of cordierite. *Journal of Metamorphic Geology* **31**(2), 187–204.

Guernina, S. & Sawyer, E. W. 2003. Large-scale melt-depletion in granulite terranes: an example from the Archaean Ashuanipi subprovince of Quebec. *Journal of Metamorphic Geology* **21**, 181–201.

Guo, L. Z., Shi, Y. S. & Lu, H. F. 1989. The pre-Devonian tectonic patterns and evolution of South China. *Journal of Southeast Asian Earth Sciences* **3**(1–4), 87–93.

Hinchey, A. M. & Carr, S. D. 2006. The S-type Ladybird leucogranite suite of southeastern British Columbia: geochemical and isotopic evidence for a genetic link with migmatite formation in the North American basement gneisses of the Monashee complex. *Lithos* **90**(3–4), 223–48.

Huang, J. Q. 1977. The basic outline of China tectonics. *Acta Geologica Sinica* **52**, 117–35.

Johannes, W., Ehlers, C., Kriegsman, L. M. & Mengel, K. 2003. The link between migmatites and S-type granites in the Turku area, southern Finland. *Lithos* **68**(3–4), 69–90.

Kong, X. S., Bao, C. M. & Gu, M. G. 1994. Discussion for main geological features and tectonic evolution of Chencai group in Zhuji district, Zhejiang Province.

Geology of Zhejiang **10**, 15–29 (in Chinese with English summary).

Kong, X., Li, Z., Feng, C., Gu, G. & Ma, J. 1995. *The Precambrian Geology of Chencai Region in Zhejiang Province*. Beijing: Precambrian Geological Publishing House, 136 pp.

Li, J. H., Dong, S. W., Zhang, Y. Q., Zhao, G. C., Johnston, S. T., Cui, J. J. & Xin, Y. 2016. New insights into Phanerozoic tectonics of South China. Part 1: polyphase deformation in the Jiuling and Lianyunshan domains of the central Jiangnan Orogen. *Journal of Geophysical Research: Solid Earth* **121**, 3048–80.

Li, L. M., Lin, S. F., Davis, D. W., Xing, G. F., Xiao, W. J. & Yin, C. Q. 2014. Geochronology and geochemistry of igneous rocks from the Kongling terrain: implications for Mesoarchean to Paleoproterozoic crustal evolution of Yangtze Block. *Precambrian Research* **255**(1), 30–47.

Li, L. M., Lin, S. F., Xing, G. F., Davis, D. W., Davis, W. J., Xiao, W. J. & Yin, C. Q. 2013a. Geochemistry and tectonic implications of late Mesoproterozoic alkaline bimodal volcanic rocks from the Tieshajie Group in the southeastern Yangtze Block, South China. *Precambrian Research* **230**, 179–92.

Li, L. M., Lin, S. F., Xing, G. F., Davis, D. W., Davis, W. J., Xiao, W. J. & Yin, C. Q. 2013b. Geochronology and geochemistry of volcanic rocks from the Shaojiwa Formation and Xingzi Group, Lushan area, SE China: implications for Neoproterozoic back-arc basin in the Yangtze Block. *Precambrian Research* **238**, 1–17.

Li, L. M., Lin, S. F., Xing, G. F., Davis, D. W., Jiang, Y., Davis, W. J. & Zhang, Y. J. 2016. Ca. 830 Ma back-arc type volcanic rocks in the eastern part of the Jiangnan Orogen: implications for the Neoproterozoic tectonic evolution of South China Block. *Precambrian Research* **275**, 209–24.

Li, L. M., Sun, M., Wang, Y. J., Xing, G. F., Zhao, G. C., Cai, K. D. & Zhang, Y. Z. 2011a. Geochronology and geochemistry of Palaeoproterozoic gneissic granites and clinopyroxenite enclaves from NW Fujian, SE China: implications for the crustal evolution of the Cathaysia Block. *Journal of Asia Earth Sciences* **41**, 204–12.

Li, L. M., Sun, M., Wang, Y. J., Xing, G. F., Zhao, G. C., He, Y. H., He, K. J. & Zhang, A. M. 2011b. U-Pb and Hf isotopic study of detrital zircons from the metasedimentary rocks in central Jiangxi Province, South China: implications for the Neoproterozoic tectonic evolution of South China Block. *Journal of Asia Earth Sciences* **41**, 44–55.

Li, L. M., Sun, M., Wang Y., J., Xing, G. F., Zhao, G. C., Lin, S. F., Xia, X. P., Chan, L. S. & Zhang, F. F. & Wong, J. 2011c. U-Pb and Hf isotopic study of zircons from migmatised amphibolites in the Cathaysia Block: implications for the early Paleozoic peak tectonothermal event in Southeastern China. *Gondwana Research* **19**, 191–201.

Li, W. X., Li, X. H., Li, Z. X. & Lou, F. S. 2008. Obduction-type granites within the NE Jiangxi Ophiolite: implications for the final amalgamation between the Yangtze and Cathaysia Blocks. *Gondwana Research* **13**, 288–301.

Li, X. H., Li, Z. X., Ge, W. C., Zhou, H. W., Li, W. X., Liu, Y. & Wingate, M. T. D. 2003. Neoproterozoic granitoids in South China: crustal melting above a mantle plume at ca825 Ma? *Precambrian Research* **122**, 45–83.

Li, X. H., Liu, Y., Li, Q. L., Guo, C. H. & Chamberlain, K. R. 2009. Precise determination of Phanerozoic zircon Pb/Pb age by multicollector SIMS without external standardization. *Geochemistry, Geophysics, Geosystems* **10**(4), Q04010. doi: 10.1029/2009GC002400.

Li, X. H., Long, W. G., Li, Q. L., Liu, Y., Zheng, Y. F., Yang, Y. H., Chamberlain, K. R., Wan, D. F., Guo, C. H., Wang, X. C. & Tao, H. 2010a. Penglai zircon megacryst: a potential new working reference for microbeam analysis of Hf-O isotopes and U-Pb age. *Geostandards and Geoanalytical Research* **34**, 117–34.

Li, X., Tang, G., Gong, B., Yang, Y., Hou, K., Hu, Z., Li, Q., Liu, Y. & Li, W. 2013b. Qinghu zircon: a working reference for microbeam analysis of U-Pb age and Hf and O isotopes. *Chinese Science Bulletin* **58**, 4647–54.

Li, Z. X., Li, X. H., Wartho, J. A., Clark, C., Li, W. X., Zhang, C. L. & Bao, C. 2010. Magmatic and metamorphic events during the early Paleozoic Wuyi-Yunkai orogeny, southeastern South China: new age constraints and pressure-temperature conditions. *Geological Society of America Bulletin* **122**, 772–93.

Li, Z. X., Wartho, J. A., Occhipinti, S., Zhang, C. L., Li, X. H., Wang, J. & Bao, C. M. 2007. Early history of the eastern Sibao Orogen (South China) during the assembly of Rodinia: new mica $^{40}Ar/^{39}Ar$ dating and SHRIMP U–Pb detrital zircon provenance constraints. *Precambrian Research* **159**, 79–94.

Lin, S. F., Brem, A. G., van Staal, C. R., Davis, D. W., McNicoll, V. J. & Pehrsson, S. 2013. The Corner Brook Lake block in the Newfoundland Appalachians: a suspect terrane along the Laurentian margin and evidence for large-scale orogen-parallel motion. *Geological Society of America Bulletin* **125**, 1618–32.

Lin, S. F., Xing, G. F., Ying, C. Q., Li, L. M., Davis, D., Davis, B., Chen, G. H., Jiang, Y. & Chen, Z. H. 2015. An Appalachian-style multi-terrane accretion/collision model for the assembly of South China. Abstract 34518 presented at 2015 Joint Assembly, AGU–GAC–MAC–CGU, Montreal, Canada, 3–7 May.

Liu, Y., Hu, Z., Zong, K., Gao, C., Gao, S., Xu, J. & Chen, H. 2010b. Reappraisement and refinement of zircon U-Pb isotope and trace element analyses by LA-ICP-MS. *Chinese Science Bulletin* **55**(15), 1535–46.

Liu, R., Zhou, H. W., Zhang, L., Zhong, Z. Q., Zeng, W., Xiang, H., Jin, S., Lu, X. Q. & Li, C. Z. 2010a. Zircon U-Pb ages and Hf isotope compositions of the Mayuan migmatite complex, NW Fujian Province, Southeast China: constraints on the timing and nature of a regional tectonothermal event associated with the Caledonian orogeny. *Lithos* **119**, 163–80.

Ludwig, K. R. 2003. *ISOPLOT 3.00: A Geochronological Toolkit for Microsoft Excel*. Berkeley, CA: Berkeley Geochronology Center.

Ma, R. S. 2006. New thought about the tectonic evolution of the South China: with discussion on several problems of the Cathyasia old land. *Geological Journal of China Universities* **12**(4), 448–56 (in Chinese with English summary).

McLaren, S., Sandiford, M. & Hand, M. 1999. High radiogenic heat-producing granites and metamorphism: an example from the western Mount Isa inlier, Australia. *Geology* **27**(8), 679–82.

McLaren, S., Sandiford, M., Powell, R., Neumann, N. & Woodhead, J. 2006. Palaeozoic intraplate crustal anatexis in the Mount Painter province, South Australia: timing, thermal budgets and the role of crustal heat production. *Journal of Petrology* **47**, 2281–302.

Molnar, P., Houseman, G. A. & Conrad, C. P. 1998. Rayleigh-Taylor instability and convective thinning of mechanically thickened lithosphere: effects of non-linear viscosity decreasing exponentially with depth and of horizontal shortening of the layer. *Geophysical Journal International* **133**, 568–84.

Montero, P., Bea, F., Zinger, T. F., Scarrow, J. H., Molina, J. F. & Whitehouse, M. 2004. 55 million years of continuous anatexis in Central Iberia: single-zircon dating of the Pena Negra Complex. *Journal of the Geological Society of London* **161**(2), 255–63.

Oliver, N. H. S., Nemchin, A. A., Bodorkos, S. & Kinny, P. D. 1999. Relationships between zircon Th-Pb-U SHRIMP isotope patterns and migmatite type in the Halls Creek orogen, Western Australia. *Journal of Petrology* **40**, 1553–75.

Qiu, Y. M., Gao, S., McNaughton, N. J., Groves, D. I. & Ling, W. 2000. First evidence of >3.2 Ga continental crust in the Yangtze craton of south China and its implications for Archean crustal evolution and Phanerozoic tectonics. *Geology* **28**, 11–14.

Sawyer, E. W. 2008. *Atlas of Migmatites*. Ontario: NRC Research Press, 371 pp. The Canadian Mineralogist, Special Publication 9.

Sawyer, E. W. 2010. Migmatites formed by water-fluxed partial melting of a leucogranodiorite protolith: microstructures in the residual rocks and source of the fluid. *Lithos* **116**, 273–86.

Scherer, E., Munker, C. & Mezger, K. 2001. Calibration of the lutetium-hafnium clock. *Science* **293**(5530), 683–7.

Shu, L. S. 2006. Predevonian tectonic evolution of South China: from Cathaysian Block to Caledonian period folded orogenic belt. *Geological Journal of China Universities* **12**(4), 418–31 (in Chinese with English summary).

Shu, L. S., Jahn, B. M., Charvet, J., Santosh, M., Wang, B., Xu, X. S. & Jiang, S. Y. 2014. Early Paleozoic depositional environment and interpolate tectonomagmatism in the Cathaysia Block (South China): evidence from stratigraphic, structural, geochemical and geochronological investigations. *American Journal of Science* **314**, 154–86.

Shu, L. S., Lu, H. F., Jia, D., Charvet, J. & Faure, M. 1999. Study of the $^{40}Ar/^{39}Ar$ isotopic age for the early Paleozoic tectonothermal event in the Wuyishan region, South China. *Journal of Nanjing University* **35**, 668–74 (in Chinese with English summary).

Shu, L. S., Yu, J. H., Jia, D., Wang, B., Shen, W. Z. & Zhang, Y. Q. 2008. Early Paleozoic orogenic belt in the eastern segment of South China. *Geological Bulletin of China* **27**, 1581–93 (in Chinese with English summary).

Shu, X. J., Wang, X. L., Sun, T., Chen, W. F. & Shen, W. Z. 2013. Crustal formation in the Nanling Range, South China Block: Hf isotope evidence of zircons from Phanerozoic granitoids. *Journal of Asian Earth Sciences* **74**, 210–24.

Shui, T. 1987. Tectonic framework of basement in Southeast China continental area. *Science in China (Series B)* **4**, 414–22 (in Chinese).

Shui, T., Xu, B. T. & Liang, R. H. 1986. The Shaoxing-Jiangshan Pangea opposite zone. *Chinese Science Bulletin* **31**(6), 444–8 (in Chinese).

Slama, J., Kosler, J., Condon, D. J., Crowley, J. L., Gerdes, A., Hanchar, J. M., Horstwood, M. S. A., Morris, G. A., Nasdala, L., Norberg, N., Schaltegger, U., Schoene, B., Tubrett, M. N. & Whitehouse, M. J. 2008. Plesovice zircon: a new natural reference material for U-Pb and Hf isotopic microanalysis. *Chemical Geology* **249**, 1–35.

Streule, M. J., Searle, M. P., Waters, D. J. & Horstwood, M. S. A. 2010. Metamorphism, melting, and channel flow in the Greater Himalayan Sequence and Makalu leucogranite: constraints from thermobarometry, metamorphic modeling, and U-Pb geochronology. *Tectonics* **29**(5), 633–50.

Stacey, J. S., Kramers, J. D. 1975. Approximation of terrestrial lead isotope evolution by a two-stage model. *Earth and Planetary Science Letters* **26**, 207–221.

Sun, S. S. & McDonough, W. F. 1989. Chemical and isotopic systematics of oceanic basalts: implications for mantle composition and processes. In *Magmatism in the Ocean Basins* (eds A. D. Saunders & M. J. Norry), pp. 313–45. Geological Society of London, Special Publication no. 42.

Voshage, H., Hofmann, A., Mazzucchelli, M., Rivalenti, G., Sinigoi, S., Raczek, I. & Demarchi, G. 1990. Isotopic evidence from the Ivrea zone for a hybrid lower crust formed by magmatic underplating. *Nature* **347**, 731–36.

Wang, C. Z., Xing, G. F., Chen, R., Hong, W. T., Zhu, Q. B., Zhao, X. L. & Jiang, Y. 2015. Zircon geochronology of the metamorphic rocks of Chencai Group in Shenzhou area, Zhejiang Province: the response of the Jiangshan-Shaoxing suture zone to the Indosinian orogenic event. *Geology in China* **42**(6), 1700–14 (in Chinese with English summary).

Wang, D., Zheng, J. P., Ma, Q., Griffin, W. L., Zhao, H. & Wong, J. 2013. Early Paleozoic crustal anatexis in the intraplate Wuyi–Yunkai orogen, South China. *Lithos* **175–176**, 124–45.

Wang, J. & Li, Z. X. 2003. History of Neoproterozoic rift basins in South China: implications for Rodinia breakup. *Precambrian Research* **122**(1–4), 141–58.

Wang, S. J., Li, S. G., Chen, L. J., He, Y. S., An, S. C. & Shen, J. 2013. Geochronology and geochemistry of leucosomes in the North Dabie Terrane, East China: implication for post-UHPM crustal melting during exhumation. *Contributions to Mineralogy and Petrology* **165**, 1009–29.

Wang, X. L., Zhou, J. C., Griffin, W. L., Wang, R. C., Qiu, J. S., O'Reilly, S. Y., Xu, X. S., Liu, X. M. & Zhang, G. L. 2007. Detrital zircon geochronology of Precambrian basement sequences in the Jiangnan orogen: dating the assembly of the Yangtze and Cathaysia Blocks. *Precambrian Research* **159**, 117–31.

Wang, X. L., Zhou, J. C., Griffin, W. L., Zhao, G. C., Yu, J. H., Qiu, J. S., Zhang, Y. J. & Xing, G. F. 2014. Geochemical zonation across a Neoproterozoic orogenic belt: isotopic evidence from granitoids and metasedimentary rocks of the Jiangnan orogen, China. *Precambrian Research* **242**, 154–71.

Wang, Y. J., Fan, W. M., Zhao, G. C., Ji, S. C. & Peng, T. P. 2007. Zircon U-Pb geochronology of gneissic rocks in the Yunkai Massif and its implications on the Caledonian event in the South China Block. *Gondwana Research* **12**, 404–16.

Wang, Y. J., Wu, C. M., Zhang, A. M., Fan, W. M., Zhang, Y. H., Zhang, Y. Z., Peng, T. P. & Yin, C. Q. 2012. Kwangsian and Indosinian reworking of the eastern South China Block: constraints on zircon U-Pb geochronology and metamorphism of amphibolite and granulite. *Lithos* **127**, 239–60.

Wang, Y. J., Zhang, A. M., Cawood, P. A., Zhang, Y. Z., Fan, W. M. & Zhang, G. W. 2013a. Geochronological

and Nd-Hf-Os geochemical fingerprinting of an early Neoproterozoic arc-back-arc system in South China and its accretionary assembly along the margin of Rodinia. *Precambrian Research* **231**, 343–71.

Wang, Y. J., Zhang, A. M., Fan, W. M., Zhang, G. W., Zhang, F. F. & Zhang, Y. Z. 2011. Kwangsian crustal anatexis within the eastern South China Block: geochemical, zircon U-Pb geochronological and Hf isotopic fingerprints from the gneissoid granites of Wugong and Wuyi-Yunkai Domains. *Lithos* **127**, 239–60.

Wang, Y. J., Zhang, A. M., Fan, W. M., Zhang, Y. H. & Zhang, Y. Z. 2013b. Origin of paleosubduction modified mantle for Silurian gabbro in the Cathaysia Block: geochronological and geochemical evidence. *Lithos* **160–161**, 37–54.

Whittington, A. & Treloar, P. 2002. Crustal anatexis and its relation to the exhumation of collisional orogenic belts, with particular reference to the Himalaya. *Mineralogical Magazine* **66**, 53–91.

Williams, I. S., Buick, I. S. & Cartwright, I. 1996. An extended episode of early Mesoproterozoic metamorphic fluid flow in the Reynolds Range, central Australia. *Journal of Metamorphic Geology* **14**(1), 29–47.

Xia, Y., Xu, X. S. & Zhu, K. Y. 2012. Paleoproterozoic S- and A-type granites in southwestern Zhejiang: magmatism, metamorphism and implications for the crustal evolution of the Cathaysia basement. *Precambrian Research* **216–219**, 177–207.

Xiang, H., Zhang, L., Zhou, H., Zhong, Z., Zeng, W., Liu, R. & Jin, S. 2008. U–Pb zircon geochronology and Hf isotope study of metamorphosed basic–ultrabasic rocks from metamorphic basement in southwestern Zhejiang: the response of the Cathaysia Block to Indosinian orogenic event. *Science in China (Series D): Earth Sciences* **51**, 788–800 (in Chinese).

Xu, B. T. 1987. Isotopic geochronology of Paleo-basement metamorphic rocks in southeastern Zhejiang Province. *Geological Review* **33**(5), 468–74 (in Chinese with English summary).

Xu, X. S., O'Reilly, S. Y., Griffin, W. L., Wang, X. L., Pearson, N. J. & He, Z. Y. 2007. The crust of Cathaysia: age, assembly and reworking of two terranes. *Precambrian Research* **158**, 51–78.

Yao, J. L, Shu, L. S. & Santosh, M. 2014. Palaeozoic metamorphism of the Neoproterozoic basement in NE Cathaysia: zircon U-Pb ages, Hf isotope and whole rock geochemistry from the Chencai Group. *Journal of the Geological Society* **171**(2), 281–97.

Yi, L. W., Ma, C. Q., Wang, L. X., Lai, Z. X., Li, X. Y., Yang, Y. N., Wu, F. & Hu, Y. R. 2014. Discovery of Late Ordovician subvolcanic rocks in South China: existence of subduction–related dacite from Early Paleozoic? Earth Science. *Journal of Geosciences*, **39**(6), 637–653. (in Chinese with English abstract)

Yu, J. H., O'Reilly, S. Y., Wang, L. J., Griffin, W. L., Zhou, M. F., Zhang, M. & Shu, L. S. 2010. Components and episodic growth of Precambrian crust in the Cathaysia Block, South China: evidence from U-Pb ages and Hf isotopes of zircons in Neoproterozoic sediments. *Precambrian Research* **181**, 97–114.

Yu, J. H., O'Reilly, S. Y., Zhou, M. F., Griffin, W. L. & Wang, L. J. 2012. U-Pb geochronology and Hf-Nd isotopic geochemistry of the Badu Complex, Southeastern China: implications for the Precambrian crustal evolution and paleogeography of the Cathaysia Block. *Precambrian Research* **222–223**, 424–49.

Yu, J. H. & Shu, L. S. 2016. Is the garnet amphibolite in the Longyou a retrograded eclogite? *Science Bulletin* **61**(6), 556–60 (in Chinese with English summary).

Yu, J. H., Wang, L. J., Griffin, W. L., O'Reilly, S. Y., Zhang, M., Li, C. Z. & Shu, L. S. 2009. A Paleoproterozoic orogeny recorded in a long-lived cratonic remnant (Wuyishan terrane), eastern Cathaysia Block, China. *Precambrian Research* **174**, 347–63.

Yu, J. H., Zhou, X. M. & O'Reilly, S. Y. 2005. Formation history and protolith characteristics of granulite facies metamorphic rock in Central Cathaysia deduced from U-Pb and Lu-Hf isotopic studies of single zircon grains. *Chinese Science Bulletin* **50**(18), 2080–9.

Yu, J. H., Zhou, X. M. & Zhao, L. 2003. Discovery and implications of granulite facies metamorphic rocks in the eastern Nanling, China. *Acta Petrologica Sinica* **19**(3), 461–7 (in Chinese with English summary).

Yuan, H. L., Gao, S., Dai, M. N., Zong, C. L., Günther, D., Fontaine, H. G., Liu, X. M. & Di Wu, C., R. 2008. Simultaneous determinations of U–Pb age, Hf isotopes and trace element compositions of zircon by excimer laser ablation quadrupole and multiple collector ICP–MS. *Chemical Geology* **247**(1–2), 100–18.

Zhang, C., Holtz, F., Koepke, J., Berndt, J. & Ma, C. Q. 2014a. Decompressional anatexis in the migmatite core complex of northern Dabie orogen, eastern China: petrological evidence and Ti-in-quartz thermobarometry. *Lithos* **202–203**, 227–36.

Zhang, C. L., Santosh, M., Zhu, Q. B., Chen, X. Y. & Huang, W. C. 2014b. The Gondwana connect of South China: evidence from monazite and zircon geochronology in the Cathaysia Block. *Gondwana Research* **28**(3), 1137–51.

Zhang, F. F., Wang, Y. J., Fan, W. M., Zhang, A. M. & Zhang, Y. Z. 2012. Geochronological and geochemical constraints on petrogenesis of the Middle Paleozoic (Kwangsian) massive granites in the eastern South China Block. *Lithos* **150**, 118–208.

Zhang, Q., Jiang, Y. H., Wang, G. C., Liu, Z., Ni, C. Y. & Qing, L. 2015. Origin of Silurian gabbros and I-type granites in central Fujian, SE China: implications for the evolution of the early Paleozoic orogen of South China. *Lithos* **216–217**, 285–97.

Zhang, S. B., Zheng, Y. F., Wu, Y. B., Zhao, Z. F., Gao, S. & Wu, F. Y. 2006. Zircon U-Pb age and Hf-O isotope evidence for Paleoproterozoic metamorphic event in South China. *Precambrian Research* **151**, 265–88.

Zhang, Z. M., Xiang, H., Dong, X., Li, W. C., Ding, H. X., Gou, Z. B. & Tian, Z. L. 2016. Oligocene HP metamorphism and anatexis of the Higher Himalayan Crystalline Sequence in Yadong region, east-central Himalaya. *Gondwana Research* **41**, published online 18 November 2016. doi: 10.1016/j.gr.2015.03.002.

Zhao, G. C. 2015. Jiangnan orogen in South China: developing from divergent double subduction. *Gondwana Research* **27**(3), 1173–80.

Zhao, G. C. & Cawood, P. A. 1999. Tectonothermal evolution of the Mayuan assemblage in the Cathaysia Block: new evidence for Neoproterozoic collisional-related assembly of the South China craton. *American Journal of Science* **299**, 309–39.

Zhao, G. C. & Cawood, P. A. 2012. Precambrian geology of China. *Precambrian Research* **222–223**, 13–54.

Zhao, G. C. & Sun, D. Y. 1994. The studies on metamorphic stages and metamorphic PTD path of Chencai Group, Southwestern Zhejiang Province. *Journal of*

Changchun Univerisity of Earth Sciences **24**(3), 246–53.

Zhao, G. C., Sun, D. Y. & He, T. X. 1994. Discussion on characteristics of structural deformations and the ages of deformations about Chencai group. *Geology of Zhejiang* **10**(1), 38–46 (in Chinese with English summary).

Zhao, L., Zhai, M. G., Zhou, X. W., Santosh, M. & Ma, X. D., 2015b. Geochronology and geochemistry of a suite of mafic rocks in Chencai area, South China: implications for petrogenesis and tectonic setting. *Lithos* **236–237**, 226–244.

Zhao, J. H., Zhou, M. F., Yan, D. P., Zheng, J. P. & Li, J. W. 2011. Reappraisal of the ages of Neoproterozoic strata in South China: no connection with the Grenvillian orogeny. *Geology* **39**, 299–302.

Zhao, L., Zhou, X. W., Zhai, M. G., Santosh, M. & Geng, Y. S. 2015a. Zircon U–Th–Pb–Hf isotopes of the basement rocks in northeastern Cathaysia block, South China: implications for Phanerozoic multiple metamorphic reworking of a Paleoproterozoic terrane. *Gondwana Research* **28**, 246–61.

Zhao, L., Zhou, X., Zhai, M., Santosh, M., Ma, X., Shan, H. & Cui, X. 2014. Paleoproterozoic tectonic transition from collision to extension in the eastern Cathaysia Block, South China: evidence from geochemistry, zircon U–Pb geochronology and Nd–Hf isotopes of a granite-charnockite suite in southwestern Zhejiang. *Lithos* **184–187**, 259–80.

Zheng, Y. F., Xiao, W. J. & Zhao, G. C. 2013. Introduction to tectonics of China. *Gondwana Research* **23**, 1189–206.

https://doi.org/10.1017/S0016756817000292 Published online by Cambridge University Press